

# Comparative study of nuclear effects in polarized electron scattering from $^3\text{He}$

J. J. Ethier<sup>1,2</sup>, W. Melnitchouk<sup>2</sup>

<sup>1</sup>*Physics Department, Stetson University, DeLand, Florida 32723*

<sup>2</sup>*Jefferson Lab, 12000 Jefferson Avenue, Newport News, Virginia 23606*

(Dated: August 22, 2018)

## Abstract

We present a detailed analysis of nuclear effects in inclusive electron scattering from polarized  $^3\text{He}$  nuclei for polarization asymmetries, structure functions and their moments, both in the nucleon resonance and deep-inelastic regions. We compare the results of calculations within the weak binding approximation at finite  $Q^2$  with the effective polarization *ansatz* often used in experimental data analyses, and explore the impact of  $\Delta$  components in the nuclear wave function and nucleon off-shell corrections on extractions of the free neutron structure. Using the same framework we also make predictions for the  $Q^2$  dependence of quasielastic scattering from polarized  $^3\text{He}$ , data on which can be used to constrain the spin-dependent nuclear smearing functions in  $^3\text{He}$ .

## I. INTRODUCTION

Reliable extraction of information on the spin structure of the neutron is vital for our understanding of the flavor and spin decomposition of the nucleon in terms of its quark and gluon constituents. When combined with the more copious measurements of the proton structure, the neutron data allow the individual  $u$  and  $d$  flavor contributions to be determined. The absence of free neutron targets, however, means that polarized nuclei such as deuterium,  $^3\text{He}$  or  $^7\text{Li}$  must be used as effective polarized neutron targets. The perennial problem of nuclear corrections must therefore be seriously addressed if one is to obtain neutron structure information with sufficient accuracy. This is especially pertinent for new generations of polarized deep-inelastic scattering (DIS) experiments that aim to measure spin structure functions and their moments with unprecedented precision [1, 2].

The study of nuclear corrections to spin structure functions in the DIS and quasi-elastic (QE) regions has some history already, with the first quantitative calculations dating back to the 1980s [3–5]. Subsequent work by Ciofi degli Atti *et al.* [6–9] and other groups [10–15] over the past two decades has made important inroads into our understanding of nuclear effects in scattering from polarized  $^3\text{He}$  nuclei, and the extraction of the spin structure of the free neutron. The technology developed for inclusive scattering has more recently been extended to other observables, such as the  $^3\text{He}$  generalized parton distributions [16] and transversity in semi-inclusive DIS [17].

While most of the traditional approaches have been based on a nonrelativistic treatment of the dynamics, some calculations of polarized  $^3\text{He}$  structure functions have attempted to incorporate relativistic and off-shell effects [18–20], although these are generally difficult to constrain unambiguously. A systematic approach for expanding the nucleon propagator in the nuclear medium was developed [21, 22] in the weak binding approximation (WBA), in which the usual convolution formulas for nuclear structure functions can be derived to order  $\mathbf{p}^2/M^2$ , where  $\mathbf{p}$  is the nucleon three-momentum and  $M$  is its mass, with identifiable higher order corrections. The WBA method was applied to polarized deuteron [23] and  $^3\text{He}$  nuclei [24], where the nuclear corrections were estimated in both the DIS and nucleon resonance regions.

The standard nuclear structure function analyses have for the most part been formulated within the plane wave impulse approximation, in which scattering is assumed to take place

incoherently from individual nucleons within the nucleus, with the closure approximation used to sum over the hadrons in the final state. Beyond the impulse approximation, nuclear shadowing corrections in polarized  ${}^3\text{He}$  have been shown to arise from multiple scattering of the lepton from two or more nucleons in the  ${}^3\text{He}$  nucleus [25, 26]. In addition, contributions to the spin-dependent  ${}^3\text{He}$  structure function from non-nucleonic degrees of freedom in the nucleus, such as the  $\Delta(1232)$  isobar, have been argued [14, 15] to account for the  $\approx 4\%$  difference between the value of the isovector axial charge  $g_A$  in the free nucleon (measured in neutron  $\beta$  decay) and that in the  $A = 3$  nuclei (from tritium  $\beta$  decay) [27].

With recent polarized  ${}^3\text{He}$  experiments at Jefferson Lab, as well as those planned for the upcoming 12 GeV energy upgrade, attaining ever greater precision, the need exists for increasingly accurate theoretical descriptions of the nuclear corrections to spin-dependent structure functions and their moments. For example, the  $d_2$  moment of the  ${}^3\text{He}$  structure functions has recently been measured in the E06-014 experiment [28] at Jefferson Lab Hall A, which can in principle reveal certain higher-twist matrix elements of the neutron — provided the nuclear corrections can be accounted for. Furthermore, extraction of the neutron polarization asymmetry  $A_1^n$  from data on the  $A_1^{{}^3\text{He}}$  asymmetry requires the simultaneous determination of nuclear corrections to the spin-dependent  $g_1$  and  $g_2$  structure functions, as well as the unpolarized  $F_1$  and  $F_2$  structure functions of  ${}^3\text{He}$ , which has not been systematically considered in previous work.

In this paper we revisit the problem of nuclear effects in inclusive scattering of polarized leptons from polarized  ${}^3\text{He}$  nuclei in the DIS, nucleon resonance and QE regions, focusing in particular on kinematics at intermediate and large values of Bjorken  $x$ . We provide a critical comparison of various approaches and approximations to computing the nuclear corrections, with a view of obtaining a more reliable estimate of the uncertainty on the nuclear effects to be used in extractions of the free neutron structure. We work within the framework of the WBA to compute the polarized nucleon light-cone momentum distributions in  ${}^3\text{He}$  (commonly referred to as “smearing functions”), and compare the full results at finite four-momentum transfer squared  $Q^2$  with those often used in the large- $Q^2$  approximation, as well as with the effective polarization *ansatz* typically adopted in experimental data analyses. In addition to the standard nuclear smearing corrections which incorporate Fermi motion and binding effects, we discuss the effects of non-nucleonic constituents of the nucleus such as the  $\Delta$  resonance, and the possible off-shell modification of the nucleon structure functions in the

nuclear medium. The effects of the various nuclear corrections are considered for both the  $g_1$  and  $g_2$  structure functions and their moments, as well as for the  $A_1$  and  $A_2$  polarization asymmetries, which requires correcting also the unpolarized  $^3\text{He}$  structure functions. As a possible test of the reliability of the nuclear corrections, we evaluate the QE contributions to the spin structure functions, which can be compared with future precision data from dedicated  $^3\text{He}$  experiments in the QE region.

This paper is organized as follows. In Sec. II we summarize the basic formulas for the inclusive cross sections, structure functions and polarization asymmetries relevant for the analysis. The formalism used for computing the polarized  $^3\text{He}$  structure functions within the WBA is outlined in Sec. III, where we discuss the full results for the nuclear smearing functions at finite values of  $Q^2$ , as well as those in the Bjorken limit and in the zero-width approximation. The latter leads to the effective polarization approximation, which is often used in analyses of  $^3\text{He}$  data. Numerical results for structure functions, asymmetries and moments are presented in Sec. IV, where we study the dependence on the nuclear wave function, and test the efficacy of the various approximations. The possible impact of effects beyond the impulse approximation, namely, from  $\Delta$  degrees of freedom and nucleon off-shell corrections, is also examined. Finally, in Sec. V we summarize our findings and discuss possible further applications of this work.

## II. CROSS SECTIONS AND ASYMMETRIES

To begin our discussion we first summarize the main formulas for cross sections and polarization asymmetries in terms of the spin-dependent  $g_1$  and  $g_2$  structure functions. The structure functions can be extracted from measurements of longitudinally polarized leptons scattered from a target that is polarized either longitudinally or transversely relative to the electron beam. For longitudinal beam and target polarization, the difference between the spin-aligned and spin-antialigned cross sections (with the arrows  $\uparrow$  and  $\uparrow\uparrow$  denoting the electron and nucleon spin orientations, respectively) is given in the target rest frame by

$$\frac{d^2\sigma^{\uparrow\downarrow}}{d\Omega dE'} - \frac{d^2\sigma^{\uparrow\uparrow}}{d\Omega dE'} = \frac{\sigma_{\text{Mott}}}{M\nu} 4 \tan^2 \frac{\theta}{2} \left[ (E + E' \cos \theta) g_1(x, Q^2) - 2Mx g_2(x, Q^2) \right], \quad (1)$$

where  $E$  and  $E'$  are the incident and scattered electron energies,  $\nu = E - E'$  is the energy transfer and  $\theta$  is the electron scattering angle. The Bjorken scaling variable is defined as

$x = Q^2/2M\nu$ , and  $\sigma_{\text{Mott}} = (4\alpha^2 E'^2/Q^4) \cos^2(\theta/2)$  is the Mott cross section for scattering from a point particle. The  $g_2$  structure function can be extracted if one in addition measures the cross section for a nucleon polarized in a direction transverse to the beam polarization,

$$\frac{d^2\sigma^{\uparrow\Rightarrow}}{d\Omega dE'} - \frac{d^2\sigma^{\uparrow\Leftarrow}}{d\Omega dE'} = \frac{\sigma_{\text{Mott}}}{M\nu} 4 \tan^2 \frac{\theta}{2} E' \sin \theta \left[ g_1(x, Q^2) + \frac{2E}{\nu} g_2(x, Q^2) \right]. \quad (2)$$

In practice, it is often easier to measure polarization asymmetries, or ratios of spin-dependent to spin-averaged cross sections. The ratios of the cross section differences in Eqs. (1) and (2) to the sums of the cross sections define the longitudinal  $A_{\parallel}$  and transverse  $A_{\perp}$  polarization asymmetries, respectively. The  $g_1$  and  $g_2$  structure functions can then be extracted from these asymmetries according to

$$g_1(x, Q^2) = F_1(x, Q^2) \frac{1}{d'} \left[ A_{\parallel} + \tan \frac{\theta}{2} A_{\perp} \right], \quad (3a)$$

$$g_2(x, Q^2) = F_1(x, Q^2) \frac{y_e}{2d'} \left[ \frac{E + E' \cos \theta}{E' \sin \theta} A_{\perp} - A_{\parallel} \right], \quad (3b)$$

where the kinematical factor  $d' = (1 - \epsilon)(2 - y_e)/[y_e(1 + \epsilon R(x, Q^2))]$ ,  $\epsilon$  is the ratio of longitudinal to transverse virtual photon polarizations, and  $y_e = \nu/E$  is the fractional energy loss of the incident electron. The ratio  $R$  is defined in terms of the spin-averaged longitudinal and transverse structure functions,

$$R(x, Q^2) = \frac{F_L(x, Q^2)}{2xF_1(x, Q^2)}, \quad (4)$$

where

$$F_L(x, Q^2) = \gamma^2 F_2(x, Q^2) - 2xF_1(x, Q^2), \quad (5)$$

with  $\gamma^2 = \mathbf{q}^2/\nu^2 = 1 + 4M^2x^2/Q^2$  and  $\mathbf{q}^2 = \nu^2 + Q^2$ . Note that the  $F_1$  structure function is related only to the transverse virtual photon coupling, while  $F_2$  is a combination of both transverse and longitudinal couplings.

One can also define virtual photon absorption asymmetries  $A_1$  and  $A_2$  in terms of the measured asymmetries,

$$A_{\parallel} = D(A_1 + \eta A_2), \quad (6a)$$

$$A_{\perp} = d(A_2 - \zeta A_1), \quad (6b)$$

where  $D = (1 - E'\epsilon/E)/(1 + \epsilon R(x, Q^2))$  is the photon depolarization factor, and the other kinematic factors are given by  $\eta = \epsilon\sqrt{Q^2}/(E - E'\epsilon)$ ,  $d = D\sqrt{2\epsilon/(1 + \epsilon)}$ , and  $\zeta = \eta(1 + \epsilon)/2\epsilon$ .

The  $A_1$  and  $A_2$  asymmetries can also be directly expressed in terms of the  $g_1$ ,  $g_2$  and  $F_1$  structure functions,

$$A_1(x, Q^2) = \frac{1}{F_1(x, Q^2)} [g_1(x, Q^2) - (\gamma^2 - 1)g_2(x, Q^2)], \quad (7a)$$

$$A_2(x, Q^2) = \frac{\sqrt{\gamma^2 - 1}}{F_1(x, Q^2)} [g_1(x, Q^2) + g_2(x, Q^2)]. \quad (7b)$$

At small values of  $x^2/Q^2$ , one then finds  $A_1 \approx g_1/F_1$ . In the same limit, the  $A_2$  asymmetry also vanishes:  $A_2 \rightarrow 0$  for  $\gamma \rightarrow 1$ . If the  $Q^2$  dependence of the polarized and unpolarized structure functions is similar, the polarization asymmetry  $A_1$  will be weakly dependent on  $Q^2$ . Furthermore, positivity constraints lead to bounds on the magnitude of the virtual photon asymmetries,

$$|A_1| \leq 1, \quad |A_2| \leq \sqrt{R}. \quad (8)$$

For QCD analysis it is usually convenient to work in terms of (Cornwall-Norton) moments of the  $g_1$  and  $g_2$  structure functions; the  $n$ -th moments are defined as

$$\Gamma_{1,2}^{(n)}(Q^2) = \int_0^1 dx x^{n-1} g_{1,2}(x, Q^2). \quad (9)$$

Note that since the moments integrate the structure functions up to  $x = 1$ , they formally include the elastic scattering contributions. The elastic contributions to  $g_1$  and  $g_2$  can be written in terms of the Sachs electric and magnetic form factors as

$$g_1^{(\text{el})}(x, Q^2) = \frac{1}{2(1 + \tau)} G_M(Q^2) (G_E(Q^2) + \tau G_M(Q^2)) \delta(x - 1), \quad (10a)$$

$$g_2^{(\text{el})}(x, Q^2) = \frac{\tau}{2(1 + \tau)} G_M(Q^2) (G_E(Q^2) - G_M(Q^2)) \delta(x - 1), \quad (10b)$$

where  $\tau = Q^2/4M^2$ . Of particular interest to the study of the nucleon's nonperturbative structure is the  $d_2$  moment,

$$d_2(Q^2) = \int_0^1 dx x^2 (2g_1(x, Q^2) + 3g_2(x, Q^2)), \quad (11)$$

which is defined so as to expose the twist-3 part of the  $g_2$  structure function. The  $g_2$  structure function is unique amongst the nucleon's structure functions in that its higher twist contributions are not suppressed by powers of  $1/Q^2$ , but enter at the same order as the twist-2 component. The latter is given by the Wandzura-Wilczek relation [29],

$$g_2^{\text{WW}}(x, Q^2) = -g_1(x, Q^2) + \int_x^1 \frac{dz}{z} g_1(z, Q^2), \quad (12)$$

where  $g_1$  here includes only twist-2 contributions. In general, the total  $d_2$  moment can be written in terms of the twist-2 (WW) and higher twist contributions,  $d_2 = d_2^{\text{WW}} + \bar{d}_2$ . Using Eq. (12) one can verify that the twist-2 part of  $d_2$  vanishes,  $d_2^{\text{WW}} = 0$ , so that measurement of  $d_2$  cleanly reveals the higher twist component  $\bar{d}_2$ . Obviously, for the WW component the lowest moment of  $g_2$  vanishes identically,  $\Gamma_2^{(1)\text{WW}} = 0$  [30].

### III. NUCLEAR STRUCTURE FUNCTIONS

In this section we present the formalism for computing the spin-dependent structure functions of  $^3\text{He}$ , and discuss their relation to the spin structure functions of the proton and neutron. Within the weak binding approximation, the nuclear and nucleon structure functions can be related by convolutions involving light-cone momentum distributions of polarized nucleons in the  $^3\text{He}$  nucleus. We consider the full results at finite  $Q^2$ , along with various approximations which arise in specific limits, as well as corrections to the convolution approximation from nucleon off-shell and non-nucleonic degrees of freedom. Coherent effects associated with multiple scattering from two or more nucleons in the nucleus give rise to corrections at small values of  $x$  [31]; in this analysis we restrict ourselves to the intermediate- and large- $x$  region,  $x \gg 0$ , in which the incoherent scattering from a single nucleon is expected to dominate.

#### A. Weak binding approximation

A systematic framework that has been used to successfully compute nuclear structure functions in terms of nucleon degrees of freedom is the weak binding approximation, in which the nucleus is treated as a nonrelativistic system of weakly bound nucleons with four-momentum  $p^\mu \equiv (M + \varepsilon, \mathbf{p})$ , with  $|\mathbf{p}|, |\varepsilon| \ll M$ . In this approach the spin-averaged  $F_{1,2}$  and spin-dependent  $g_{1,2}$  structure functions of nuclei have been derived by Kulagin *et al.* in Refs. [21–24, 32]. Neglecting possible nucleon structure modifications off the mass shell (see Sec. IIID below), the spin-dependent structure functions of  $^3\text{He}$  can be written, to order  $\mathbf{p}^2/M^2$ , as [22–24]

$$g_i^{^3\text{He}}(x, Q^2) = \int \frac{dy}{y} \left[ 2f_{ij}^p(y, \gamma) g_j^p\left(\frac{x}{y}, Q^2\right) + f_{ij}^n(y, \gamma) g_j^n\left(\frac{x}{y}, Q^2\right) \right], \quad i, j = 1, 2, \quad (13)$$

where  $y = p \cdot q / M\nu = (M + \varepsilon + \gamma p_z) / M$  is the nuclear light-cone momentum fraction carried by the interacting nucleon, and a sum over indices  $j$  is implied. The functions  $f_{ij}^N(y, \gamma)$  are nucleon light-cone momentum distributions (or “smearing functions”) in the  ${}^3\text{He}$  nucleus computed in terms of the nuclear spectral function,

$$f_{ij}^N(y, \gamma) = \int \frac{d^4p}{(2\pi)^4} D_{ij}^N(\varepsilon, \mathbf{p}, \gamma) \delta\left(y - 1 - \frac{\varepsilon + \gamma p_z}{M}\right), \quad (14)$$

with  $N = p$  or  $n$ . In the Bjorken limit ( $\gamma \rightarrow 1$ ), the smearing functions depend only on the light-cone momentum fraction  $y$ , which spans the range between  $x$  and  $M_{\text{He}}/M \approx 3$ . At finite  $Q^2$ , however, they depend in addition on the variable  $\gamma$ , making them process-dependent at finite kinematics.

The energy-momentum distribution functions  $D_{ij}^N$  can be conveniently expressed in terms of coefficients of the spectral function  $\mathcal{P}^N$  [11],

$$\mathcal{P}^N(\varepsilon, \mathbf{p}, S) = \frac{1}{2} \left[ \mathcal{F}_0^N + \mathcal{F}_\sigma^N \boldsymbol{\sigma} \cdot \mathbf{S} + \mathcal{F}_t^N (\hat{\mathbf{p}} \cdot \mathbf{S} \hat{\mathbf{p}} \cdot \boldsymbol{\sigma} - \frac{1}{3} \mathbf{S} \cdot \boldsymbol{\sigma}) \right], \quad (15)$$

where  $\hat{\mathbf{p}}$  is a unit vector in the direction of  $\mathbf{p}$ , and the nuclear spin vector  $\mathbf{S}$  is defined to lie along the  $z$ -axis. The spectral coefficient  $\mathcal{F}_0^N$  represents the spin-averaged distribution of nucleons in the nucleus, while the spin-dependent distributions are parametrized in terms of the longitudinal  $\mathcal{F}_\sigma^N$  and tensor  $\mathcal{F}_t^N$  spectral coefficients. In general, the spectral coefficients are functions of the separation energy  $\varepsilon$  and the magnitude  $|\mathbf{p}|$  of the nucleon momentum,  $\mathcal{F}_{0,\sigma,t}^N \equiv \mathcal{F}_{0,\sigma,t}^N(\varepsilon, |\mathbf{p}|)$ . For the  $g_1$  structure function the nucleon energy-momentum distributions are given by [22–24]

$$D_{11}^N = \mathcal{F}_\sigma^N + \frac{3 - \gamma^2}{6\gamma^2} (3\hat{p}_z^2 - 1) \mathcal{F}_t^N + \frac{p_z}{\gamma M} (\mathcal{F}_\sigma^N + \frac{2}{3} \mathcal{F}_t^N) + \frac{\mathbf{p}^2}{M^2} \frac{(3 - \gamma^2)\hat{p}_z^2 - 1 - \gamma^2}{12\gamma^2} (3\mathcal{F}_\sigma^N - \mathcal{F}_t^N), \quad (16a)$$

$$D_{12}^N = (\gamma^2 - 1) \left[ -\frac{3\hat{p}_z^2 - 1}{2\gamma^2} \mathcal{F}_t^N + \frac{p_z}{\gamma M} (\mathcal{F}_\sigma^N + (\frac{3}{2}\hat{p}_z^2 - \frac{5}{6}) \mathcal{F}_t^N) - \frac{\mathbf{p}^2}{M^2} \left( \frac{1 + \hat{p}_z^2(4\gamma^2 - 3)}{4\gamma^2} \mathcal{F}_\sigma^N + \frac{5 + 18\hat{p}_z^4\gamma^2 - 5\hat{p}_z^2(3 + 2\gamma^2)}{12\gamma^2} \mathcal{F}_t^N \right) \right], \quad (16b)$$



while for the  $g_2$  structure function the corresponding distributions are

$$D_{21}^N = -\frac{3\widehat{p}_z^2 - 1}{2\gamma^2} \mathcal{F}_t^N - \frac{p_z}{\gamma M} (\mathcal{F}_\sigma^N + \frac{2}{3} \mathcal{F}_t^N) - \frac{\mathbf{p}^2}{M^2} \frac{3\widehat{p}_z^2 - 1}{12\gamma^2} (3\mathcal{F}_\sigma^N - \mathcal{F}_t^N), \quad (16c)$$

$$D_{22}^N = \mathcal{F}_\sigma^N + \frac{2\gamma^2 - 3}{6\gamma^2} (3\widehat{p}_z^2 - 1) \mathcal{F}_t^N + \frac{p_z}{\gamma M} [(1 - \gamma^2) \mathcal{F}_\sigma^N + (-\frac{5}{6} + \frac{1}{3}\gamma^2 + \widehat{p}_z^2(\frac{3}{2} - \gamma^2)) \mathcal{F}_t^N] \\ + \frac{\mathbf{p}^2}{M^2} \left[ \frac{\widehat{p}_z^2(3 - 6\gamma^2 + 4\gamma^4) - 1 - 2\gamma^2}{4\gamma^2} \mathcal{F}_\sigma^N + \frac{5 - 2\gamma^2(1 + 3\widehat{p}_z^2) + 4\widehat{p}_z^2\gamma^4}{12\gamma^2} (3\widehat{p}_z^2 - 1) \mathcal{F}_t^N \right]. \quad (16d)$$

Note that in the  $\gamma \rightarrow 1$  limit, the  $D_{12}^N$  function vanishes, in which case the nuclear  $g_1$  structure function receives contributions only from  $g_1^N$ . On the other hand, both  $g_1^N$  and  $g_2^N$  contribute to the nuclear  $g_2$  structure function at all  $Q^2$  values. For  $\gamma = 1$ , the diagonal functions  $f_{11}^N$  and  $f_{22}^N$  integrate to the effective nucleon polarizations (see Sec. III B below), while the integral over the off-diagonal  $f_{21}^N$  smearing function vanishes. The dependence of the smearing functions  $f_{ij}^N$  on  $y$  and  $\gamma$  is illustrated in Ref. [24] for realistic models of the  $^3\text{He}$  spectral function.

The integrated spectral function coefficient  $\mathcal{F}_\sigma^N$  determines the average nucleon polarization in the nucleus,

$$\langle \sigma_z \rangle^N = \int \frac{d^4p}{(2\pi)^4} \mathcal{F}_\sigma^N, \quad (17)$$

while  $\mathcal{F}_t^N$  is related to the tensor polarization [11, 24]. For  $^3\text{He}$ , the integral of the function  $\mathcal{F}_0$  gives the number of protons (2) or neutrons (1) in the nucleus. The average nucleon polarization can also be written in more familiar notation in terms of the probabilities of the nucleons in the  $^3\text{He}$  nucleus to be in relative  $S$ ,  $S'$  or  $D$  states [33],

$$\langle \sigma_z \rangle^p = -\frac{2}{3} (P_D - P_{S'}), \quad (18a)$$

$$\langle \sigma_z \rangle^n = P_S - \frac{1}{3} (P_D - P_{S'}). \quad (18b)$$

Typically, the space-symmetric  $S$ -state is the dominant contribution, with the  $L = 0$  mixed-symmetric  $S'$  state and  $L = 2$  tensor  $D$ -state giving small corrections [33].

## B. Effective polarizations

In the limit of zero nuclear binding and  $\gamma \rightarrow 1$ , the smearing functions become infinitesimally narrow ( $f_{ii}^N \sim \delta(1 - y)$ , with  $f_{i \neq j}^N = 0$ ), resulting in nuclear corrections that are

independent of  $x$ . In this approximation one can express the nuclear structure functions as linear combinations of the proton and neutron structure functions weighted by effective polarizations  $P_i^N$ ,

$$g_i^{3\text{He}}(x, Q^2) = 2P_i^p g_i^p(x, Q^2) + P_i^n g_i^n(x, Q^2), \quad i = 1, 2. \quad (19)$$

The proton effective polarizations  $P_i^p$  are defined to be the *average* polarizations of the two protons in the  $^3\text{He}$  nucleus, rather than the total proton polarization. The effective polarizations are defined in terms of integrals of the diagonal smearing functions  $f_{11}^N$  and  $f_{22}^N$  at  $\gamma = 1$ ,

$$P_i^N = \int dy f_{ii}^N(y, \gamma = 1), \quad (20)$$

which can be expressed through the momentum-weighted moments  $\mathcal{F}_m^{N(n)}$  of the spectral coefficients,

$$P_1^N = \mathcal{F}_\sigma^{N(0)} - \frac{1}{3} \left( \mathcal{F}_\sigma^{N(2)} - \frac{1}{3} \mathcal{F}_t^{N(2)} \right), \quad (21a)$$

$$P_2^N = \mathcal{F}_\sigma^{N(0)} - \frac{2}{3} \left( \mathcal{F}_\sigma^{N(2)} - \frac{1}{15} \mathcal{F}_t^{N(2)} \right), \quad (21b)$$

with

$$\mathcal{F}_m^{N(n)} \equiv \int \frac{d^4p}{(2\pi)^4} \left( \frac{\mathbf{p}}{M} \right)^n \mathcal{F}_m^N(\varepsilon, \mathbf{p}), \quad m = 0, \sigma, t. \quad (22)$$

In this notation the average nucleon polarization in Eq. (17) can also be written as  $\langle \sigma_z \rangle^N \equiv \mathcal{F}_\sigma^{N(0)}$ .

The effective polarizations can be computed numerically from models of the  $^3\text{He}$  wave function. Table I lists values of the coefficients in Eqs. (21) for the proton and neutron obtained from the spectral function of Kievsky *et al.* (KPSV) [12], which is calculated using a variational approach with a pair-correlated hyperspherical-harmonic basis. For comparison, we also list values (in parentheses) obtained from the spectral function of Schulze and Sauer (SS) [11], which uses the trinucleon bound-state wave function from Ref. [34] computed by solving the Faddeev equations for 18 channels.

The lowest order neutron coefficient  $\langle \sigma_z \rangle^n$  dominates all other contributions, giving an average neutron polarization of  $\approx 86\%$  (89%) for the KPSV (SS) spectral function. The small negative value of the average proton polarization reflects the preferential antialignment of

TABLE I: Effective polarization parameters  $\mathcal{F}_\sigma^{N(0)}$ ,  $\mathcal{F}_\sigma^{N(2)}$ ,  $\mathcal{F}_t^{N(2)}$  and the average polarizations  $P_1^N$  and  $P_2^N$  for the neutron and proton, from the KPSV [12] and SS [11] (in parentheses) spectral functions.

	$\mathcal{F}_\sigma^{N(0)}$	$\mathcal{F}_\sigma^{N(2)}$	$\mathcal{F}_t^{N(2)}$	$P_1^N$	$P_2^N$
neutron	0.856	0.018	0.013	0.851	0.844
	(0.888)	(0.016)	(0.010)	(0.884)	(0.878)
proton	-0.029	-0.002	0.009	-0.028	-0.028
	(-0.022)	(-0.001)	(0.004)	(-0.021)	(-0.021)

the spins of the proton pair, with  $\langle\sigma_z\rangle^p \approx -3\%(-2\%)$  for the two models. Other models, such as the PEST three-body wave function [13], give similar values,  $\langle\sigma_z\rangle^n = 88\%$  and  $\langle\sigma_z\rangle^p = -2\%$ , as does an earlier world average of three-nucleon models,  $\langle\sigma_z\rangle^n = 86 \pm 2\%$  and  $\langle\sigma_z\rangle^p = -2.8 \pm 0.4\%$  [33].

The  $\mathbf{p}^2$ -weighted moment  $\mathcal{F}_\sigma^{N(2)}$  is  $\approx 2\%$  of the average polarization for the neutron and  $\approx 3-4\%$  for the proton. The  $\mathbf{p}^2$ -weighted tensor moment  $\mathcal{F}_t^{N(2)}$  is  $\approx 1\%-1.5\%$  of the leading  $\mathcal{F}_\sigma^{N(0)}$  term for the neutron, but a somewhat larger fraction,  $\approx 10\% - 15\%$ , for the proton, and with opposite sign (although, as noted, the proton average polarization itself is very small). In practice, the additional suppression factors of  $\sim 10$  and  $\sim 20$  for the  $P_1^N$  and  $P_2^N$  effective polarization in Eqs. (21), respectively, render the tensor contributions negligible. Overall, the higher order coefficients reduce the magnitude of the neutron polarization by  $\approx 1\% - 1.5\%$ , and the proton polarization by  $\approx 2\% - 3\%$ . On the scale of the nuclear wave function model dependence [11, 12] of the effective polarizations, which amounts to  $\sim 4\%$  for the neutron and  $\sim 15\%$  for the proton, the higher order corrections are not significant.

### C. Non-nucleonic contributions

While scattering from nucleons in the nucleus gives the dominant contribution to nuclear DIS, there are indications that a description of nuclear properties in terms of nucleon degrees of freedom alone may not be complete. Pions and vector mesons have long been recognized as playing an important role in the structure and interactions of nucleons at low energies, and their effects may also be relevant in high energy reactions such as DIS. A notable example is the nuclear EMC effect, or the ratio of nuclear to deuteron structure functions, which

deviates from unity due to the redistribution of momentum between nucleons and pions in the nucleus [35]. DIS from pions and other mesons exchanged between different nucleons in the nucleus can also lead to antishadowing effects at  $x \sim 0.1$  in unpolarized structure functions [36–38]. More recently, it was observed [39] that the presence of an isovector-vector  $\rho^0$  mean field in asymmetric nuclei can induce a shift in the  $u$  and  $d$  quark distributions which has important consequences for the NuTeV anomaly.

For spin-dependent observables, a small admixture of the  $\Delta(1232)$  isobar in the three-body wave function [40] was found to be necessary to understand the experimental value of the axial vector charge measured in  ${}^3\text{H}$   $\beta$  decay [27]. The same mechanism was argued [14, 25] to contribute also to the isovector  $g_1$  structure function for the  ${}^3\text{He}$ – ${}^3\text{H}$  system, whose lowest moment is given by the Bjorken sum rule [41]

$$\frac{\Gamma_1^{3\text{H}(1)} - \Gamma_1^{3\text{He}(1)}}{\Gamma_1^{p(1)} - \Gamma_1^{n(1)}} = \frac{g_A^{3\text{H}}}{g_A}. \quad (23)$$

Experimentally, one finds an  $\approx 4\%$  suppression of the axial vector charge for  ${}^3\text{H}$  compared with the nucleon,  $g_A^{3\text{H}}/g_A = 0.956 \pm 0.004$  [27]. Neglecting the Fermi motion of the  $\Delta$  baryon in the nucleus, the  $\Delta$  contribution to the nuclear  $g_1$  structure function was incorporated by Bissey *et al.* [13] in terms of off-diagonal  $N \rightarrow \Delta$  transition structure functions and corresponding effective polarizations  $P_1^{N\Delta}$ . For a  ${}^3\text{He}$  target, the total  $g_1$  structure function is then given by

$$g_1^{3\text{He}}(x, Q^2) = g_1^{3\text{He}}(x, Q^2)\Big|_N + g_1^{3\text{He}}(x, Q^2)\Big|_\Delta, \quad (24)$$

where the nucleonic contribution  $g_1^{3\text{He}}(x, Q^2)\Big|_N$  is given by Eq. (13) (or the effective polarization approximation, Eq. (19)), and

$$g_1^{3\text{He}}(x, Q^2)\Big|_\Delta = 2 \left[ P_1^{n\Delta^0} g_1^{n\Delta^0}(x, Q^2) + P_1^{p\Delta^+} g_1^{p\Delta^+}(x, Q^2) \right]. \quad (25)$$

In valence quark models the nucleon  $g_1$  structure function can be decomposed into contributions involving scalar and axial vector spectator diquarks [42, 43], which allows the transition structure functions to be related by [13]

$$g_1^{n\Delta^0}(x, Q^2) = g_1^{p\Delta^+}(x, Q^2) = \frac{2\sqrt{2}}{5} [g_1^p(x, Q^2) - 4g_1^n(x, Q^2)]. \quad (26)$$

The effective transition polarizations can then be determined from Eqs. (23)–(26) in terms of the diagonal polarizations  $P_1^N$  and the moments  $\Gamma_1^{N(1)}$  of the nucleon  $g_1$  structure functions,

$$P_1^{n\Delta^0} + P_1^{p\Delta^+} = \frac{5}{4\sqrt{2}} \frac{(P_1^n - P_1^p - g_A^{3\text{H}}/g_A)(\Gamma_1^{p(1)} - \Gamma_1^{n(1)})}{\Gamma_1^{p(1)} - 4\Gamma_1^{n(1)}}. \quad (27)$$

Using the most recent de Florian *et al.* (DSSV) [44] parametrization of the spin-dependent parton distribution functions (PDFs) at  $Q^2 = 5 \text{ GeV}^2$  and the KPSV values for the effective polarizations [12], we find  $P_1^{n\Delta^0} + P_1^{p\Delta^+} = -0.0125$ . This can be compared with the value  $-0.012$  obtained by Bissey *et al.* [13] using the earlier GRSV spin-dependent PDFs [45], and including corrections from nucleon off-shell effects [46] (see Sec. III D below).

For the  $g_2$  structure function, there is no corresponding isovector sum rule analogous to the Bjorken sum rule. However, in the WW (leading twist) approximation, and in the absence of nuclear Fermi motion, the  $\Delta$  contributions to  $g_2^{3\text{He}}$  can be expressed in analogy with those for  $g_1^{3\text{He}}$  in Eq. (25), which we shall use in our numerical estimates in Sec. IV.

#### D. Nucleon off-shell corrections

In the derivation of the one-dimensional convolution representation of the nuclear structure function in Eq. (13), the partonic structure of the free nucleon was assumed to be unaltered when the nucleon is placed inside the nucleus. Off-shell dependence of the nucleon structure functions would require a generalization of (13) to take into account the additional dependence of  $g_{1,2}^N$  on  $p^2 \neq M^2$ . In the WBA, to order  $\mathbf{p}^2/M^2$  in the nucleon momentum, one can write a generalized, two-dimensional convolution for the nuclear structure function in terms of a  $y$ - and  $p^2$ -dependent smearing function and a ( $p^2$ -dependent) off-shell nucleon structure function [22]

$$g_i^{3\text{He}}(x, Q^2) = \int \frac{dy}{y} \int dp^2 \left[ 2\tilde{f}_{ij}^p(y, \gamma, p^2) g_j^p\left(\frac{x}{y}, Q^2, p^2\right) + \tilde{f}_{ij}^n(y, \gamma, p^2) g_j^n\left(\frac{x}{y}, Q^2, p^2\right) \right], \quad (28)$$

where  $i, j = 1, 2$  and the off-shell dependent smearing function is defined in analogy with that in Eq. (14) by

$$\tilde{f}_{ij}^N(y, \gamma, p^2) = \int \frac{d^4p}{(2\pi)^4} D_{ij}^N(\varepsilon, \mathbf{p}, \gamma) \delta\left(y - 1 - \frac{\varepsilon + \gamma p_z}{M}\right) \delta(p^2 - (M + \varepsilon)^2 + \mathbf{p}^2). \quad (29)$$

The presence of the  $p^2$  dependence in the nucleon structure functions in Eq. (28) does not allow the  $y$  and  $p^2$  integrations to decouple, as in the on-shell convolution expression (13). Note that from Eqs. (14) and (29), the smearing function  $f_{ij}^N(y, \gamma)$  is obtained simply by integrating the off-shell function  $\tilde{f}_{ij}^N(y, p^2, \gamma)$  over  $p^2$ ,

$$f_{ij}^N(y, \gamma) = \int dp^2 \tilde{f}_{ij}^N(y, \gamma, p^2). \quad (30)$$

The dependence of the bound nucleon structure function on the off-shell mass  $p^2$  is generally difficult to determine. In fact, the concept of nucleon off-shell effects is inherently a theoretical construct which is strictly defined only within a specific definition of the nucleon fields; field redefinitions can in principle be made to move strength between wave function and off-shell contributions, with only the total structure function being physical. For the case of the deuteron structure function, this was demonstrated for both unpolarized and polarized scattering in Refs. [18, 19, 47] in a simple spectator quark model. A number of other models have also been considered in attempts to quantify the possible modification of the nucleon substructure in the nuclear medium [32, 46, 48–52].

In the WBA, the average nuclear binding and kinetic energies of the in-medium nucleons are small compared with the nucleon mass, so that the typical nucleon virtuality is  $|p^2 - M^2|/M^2 \ll 1$ . In this case, the bound nucleon structure function can be expanded in a Taylor series about the on-shell limit [22],

$$g_i^N(x, Q^2, p^2) = g_i^N(x, Q^2) + (p^2 - M^2) \left. \frac{\partial g_i^N}{\partial p^2} \right|_{p^2=M^2}. \quad (31)$$

To determine the  $p^2$  derivative of the off-shell structure functions, we take the leading twist approximation for  $g_1^N$  and  $g_2^N$ , and assume that the spin-dependent quark distribution at a scale  $Q^2 = Q_0^2$  can be written in the form of a spectral representation,

$$\Delta q(x, p^2) = \int ds \int_{-\infty}^{k_{\max}^2(x, p^2)} dk^2 \rho(s, x, p^2, k^2), \quad (32)$$

where  $k$  is the four-momentum of the interacting quark, with maximum virtuality  $k_{\max}^2 = x(p^2 - s)/(1 - x)$ , and  $s = (p - k)^2$  is the invariant mass squared of the spectator quark system. Since our focus is mainly on the nuclear effects in the large- $x$  region, we consider the application of the model specifically to the spin-dependent valence quark PDFs. In this case the quark spectral function may be approximation by a single pole at mass  $s = s_0$  [32],

$$\rho \rightarrow \delta(s - s_0) \Phi(k^2, p^2). \quad (33)$$

Fits to the free nucleon structure functions in the valence quark region suggest values of the invariant spectator masses squared  $\sim 2 \text{ GeV}^2$  [32], and in practice we use  $s_0 = 2.1 \text{ GeV}^2$ . Following Refs. [32, 51], the off-shell dependence of the quark spectral function can be parametrized through the  $p^2$  dependence of the ultraviolet cutoff parameter  $\Lambda_N(p^2)$  used to regulate the  $k^2$  integration in Eq. (32). The cutoff  $\Lambda_N$  can be related to the radius

of confinement of the nucleon  $R_N$ ,  $\Lambda_N \sim 1/R_N$ , with the variation with  $p^2$  reflecting the amount of nucleon swelling in the nuclear medium. From the analysis of the nuclear EMC effect in the  $Q^2$  rescaling model [53], typical values for nucleon swelling in the  ${}^3\text{He}$  nucleus were found to be  $\delta R_N/R_N \approx 4.0\% - 4.7\%$ .

Within this framework, the  $p^2$  derivative of the spin-dependent structure function  $g_i^N$  becomes

$$M^2 \left. \frac{\partial g_i^N}{\partial p^2} \right|_{p^2=M^2} = c_N g_i^N + h_N(x) \frac{\partial g_i^N}{\partial x}, \quad (34)$$

where

$$h_N(x) = x(1-x) \frac{(1-\lambda_N)(1-x)M^2 + \lambda_N s_0}{(1-x)^2 M^2 - s_0}. \quad (35)$$

The scale parameter  $\lambda_N$  is the  $p^2$  derivative of the cutoff  $\Lambda_N$ , and can be expressed in terms of the change in confinement scale  $\delta R_N/R_N$  and the average virtuality of the nucleon  $\langle \delta p^2 \rangle_N$ ,

$$\lambda_N \equiv \left. \frac{\partial \ln \Lambda_N^2}{\partial \ln p^2} \right|_{p^2=M^2} = -2 \frac{\delta R_N/R_N}{\langle \delta p^2 \rangle_N / M^2}, \quad (36)$$

where

$$\langle \delta p^2 \rangle_N = \int dy dp^2 (p^2 - M^2) \tilde{f}_0^N(y, p^2, \gamma). \quad (37)$$

Here the function  $\tilde{f}_0^N$  is the spin-averaged analog of the off-shell nucleon smearing functions in  ${}^3\text{He}$ . Note that because the proton and neutron momentum distributions in  ${}^3\text{He}$  are not identical, the average value of the virtuality of the bound proton and neutron in  ${}^3\text{He}$  will in general be different. Using the KPSV spectral function, the average virtualities for the proton and neutron are  $\langle \delta p^2 \rangle_n / M^2 \approx -9.5\%$  and  $\langle \delta p^2 \rangle_p / M^2 \approx -7.2\%$ , respectively. (For comparison, the corresponding average virtuality of nucleons in a deuterium nucleus is  $\approx -(4-6)\%$  [51].)

For spin-averaged PDFs, the normalization coefficient  $c_N$  in Eq. (34) was computed in Ref. [51] by requiring that the off-shell corrections do not modify the valence quark number, while Kulagin and Petti [32] imposed the sum of the off-shell and shadowing corrections to not renormalize the valence quark number. For the axial vector current, there is no corresponding sum rule for a bound nucleon; however, it is reasonable to assume a similar invariance of the axial charge for a given flavor  $q$  in the nuclear medium. As discussed in Sec. III C above, the axial vector charge in the  $\beta$  decay of  ${}^3\text{H}$  differs by  $\approx 4\%$  from that in

neutron  $\beta$  decay, and some of this difference could arise from nucleon off-shell corrections [13]. In the framework of the present analysis, the entire difference is attributed to wave function effects and corrections arising from  $\Delta$  components in the nuclear wave function [40], so that off-shell corrections do not modify the lowest moments of the valence quark PDFs. This assumption is equivalent to the condition

$$\int_0^1 dx \left. \frac{\partial g_i^N}{\partial p^2} \right|_{p^2=M^2} = 0, \quad (38)$$

which leads to the constraint on the normalization constant

$$c_N = -\frac{\int_0^1 dx h_N(x) (\partial g_i^N / \partial x)}{\Gamma_i^{N(1)}}. \quad (39)$$

In the following we will refer to this model as the off-shell covariant spectator (OCS) model.

In a somewhat different framework, Steffens *et al.* [46] used the quark-meson coupling (QMC) model to compute the effects of mean field potentials in the nucleus using the local density approximation. The in-medium scalar ( $\sigma$ ) and vector ( $\rho, \omega$ ) fields modify the quark-meson couplings, inducing changes in the nucleon's mass and energy, as well as the energy of intermediate state. For the quark distributions in the free nucleon the MIT bag model was used, which restricts the validity of the calculation to  $0.2 \lesssim x \lesssim 0.7$ . The net effect is a small, flavor-dependent correction, which was parametrized in terms of the ratio of the PDFs in the free and bound nucleons,

$$\frac{\Delta q_v(x)}{\Delta \tilde{q}_v(x)} = a_q x^{b_q} + c_q x^{d_q} (1-x)^{e_q}, \quad (40)$$

with the parameters  $a_q, \dots, e_q$  given in Ref. [46] for the  ${}^3\text{He}$  and  ${}^6\text{Li}$  nuclei. In the next section we compare the effects of these models on the  $g_1^{{}^3\text{He}}$  structure function and estimate the uncertainty arising from the off-shell model dependence.

#### IV. NUMERICAL RESULTS

In this section we present the numerical results for the various spin-dependent nuclear corrections described in Sec. III. We consider the effects on the  $x$  dependence of the  $g_1$  and  $g_2$  structure functions of  ${}^3\text{He}$ , and several of their low moments, as well as on the polarization asymmetries that are more directly accessed in inclusive scattering experiments. In particular, we study the impact of the different corrections and their uncertainties on the



extraction of the spin structure of the neutron, and the accuracy of the various approximations used in the literature. We examine the corrections in both the DIS and nucleon resonance regions, using, for illustration, the DSSV [44] leading twist parametrization of the spin-dependent PDFs in the former, and the MAID parametrization for the low- $W$  region. To estimate the dependence of the results on the input nucleon parametrization, we also compare with the parametrization from Ref. [54]. For the nucleon distributions in  $^3\text{He}$ , we use the spin-dependent KPSV spectral function [12], but consider also the results with the SS [11] spectral function.

### A. Structure Functions

To begin our discussion of the nuclear effects on the  $^3\text{He}$  structure functions and polarization asymmetries, we note that since the latter are ratios of spin-averaged to spin-dependent structure functions, they will in general also depend on the nuclear corrections in the unpolarized  $F_1$  and  $F_2$  structure functions. To determine the role played by nuclear effects in the asymmetries, it is therefore necessary to first understand the corrections to the  $^3\text{He}$   $F_1$  and  $F_2$  structure functions.

In Fig. 1 the spin-averaged  $F_1$  and  $F_2$  structure functions for  $^3\text{He}$  are compared with those for the corresponding nucleon isospin combination,  $2p + n$ , at  $Q^2 = 1$  and  $5 \text{ GeV}^2$ . Note that at finite  $Q^2$  the nuclear  $F_1$  structure function receives contributions from the nucleon  $F_1$  and  $F_2$  structure functions, while the nuclear  $F_2$  structure functions depends only on  $F_2^N$  at any  $Q^2$ . At the lower  $Q^2$  value, the resonance structures are prominent at large values of  $x$  for the free proton and neutron structure functions, particularly in the region of the  $\Delta(1232)$  resonance. For the input nucleon  $F_1$  and  $F_2$  structure functions we use the resonance parametrization of Bosted and Christy [55]. After applying the nuclear smearing corrections in the WBA, using the spin-averaged analogs [32] of the nucleon momentum distribution functions  $f_{ij}^N$  in Sec. III A with the KPSV spectral functions, the resonance peaks are significantly smeared out. The effects is strongest in the  $\Delta$  region, where the smearing reduces the height of the peaks by a factor of  $\approx 2$ .

This is also evident in the ratio of the  $^3\text{He}$  to  $2p+n$  structure functions shown in Fig. 1(b), where the resonance structures are effectively inverted compared to those in the  $F_1$  and  $F_2$  functions themselves. In contrast, the ratios of the  $^3\text{He}$  to nucleon structure functions in the

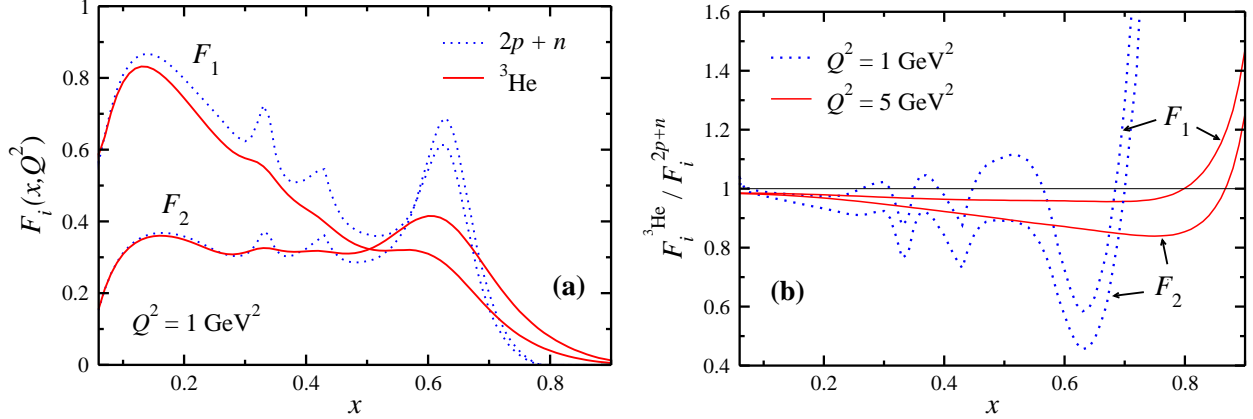


FIG. 1: **(a)** Spin-averaged  $F_1$  and  $F_2$  structure functions of  ${}^3\text{He}$  (solid) and  $(2p+n)$  (dotted), using the Bosted-Christy nucleon structure function parametrization [55] at  $Q^2 = 1 \text{ GeV}^2$ . **(b)** Ratios of  $F_1$  and  $F_2$  structure functions of  ${}^3\text{He}$  to  $(2p+n)$  at  $Q^2 = 1 \text{ GeV}^2$  (dotted) and  $Q^2 = 5 \text{ GeV}^2$  (solid), using the BC [55] and NMC [56] nucleon structure function parametrization for the resonance and DIS regions, respectively. The  ${}^3\text{He}$  structure functions in all cases are computed using the convolution formalism including finite  $Q^2$  corrections [32].

deep-inelastic region at  $Q^2 = 5 \text{ GeV}^2$ , computed using the NMC parametrization [56], show the smooth behavior characteristic of the nuclear EMC effect, with a depletion at  $x \sim 0.7$  and a subsequent rise above unity at larger  $x$  due to Fermi motion.

Qualitatively similar effects of smearing are observed for the spin-dependent  ${}^3\text{He}$  structure functions  $g_1$  and  $g_2$  in Fig. 2. Here the functions  $xg_1$  and  $xg_2$  for the free neutron are compared with the corresponding  ${}^3\text{He}$  functions computed using the various approximations discussed in Sec. III, both in the resonance region at  $Q^2 = 1 \text{ GeV}^2$  (Figs. 2(a) and (b)) and in the DIS region at  $Q^2 = 5 \text{ GeV}^2$  (Figs. 2(c) and (d)). In particular, we compute the  ${}^3\text{He}$  structure functions using the effective polarization approximation (EPA), Eq. (19), including the effects of  $\Delta$  components in the nuclear wave function, Eq. (25), and accounting for Fermi smearing effects, both in the Bjorken limit ( $\gamma = 1$ ) and at finite  $Q^2$ , Eq. (28).

For the input nucleon structure functions we use the MAID model [57] for the resonance region at low  $W$  values, and the DSSV leading twist parametrization [44] in the DIS region, which is taken here to be  $W^2 \geq 3 \text{ GeV}^2$ . At  $Q^2 = 1 \text{ GeV}^2$ , the boundary between these (indicated by the dashed vertical lines in Figs. 2(a) and (b)), occurs at  $x \approx 0.32$ . At this  $Q^2$  the dominant feature in the structure functions is the strong  $\Delta$  resonance peak at  $x \approx 0.6$ .

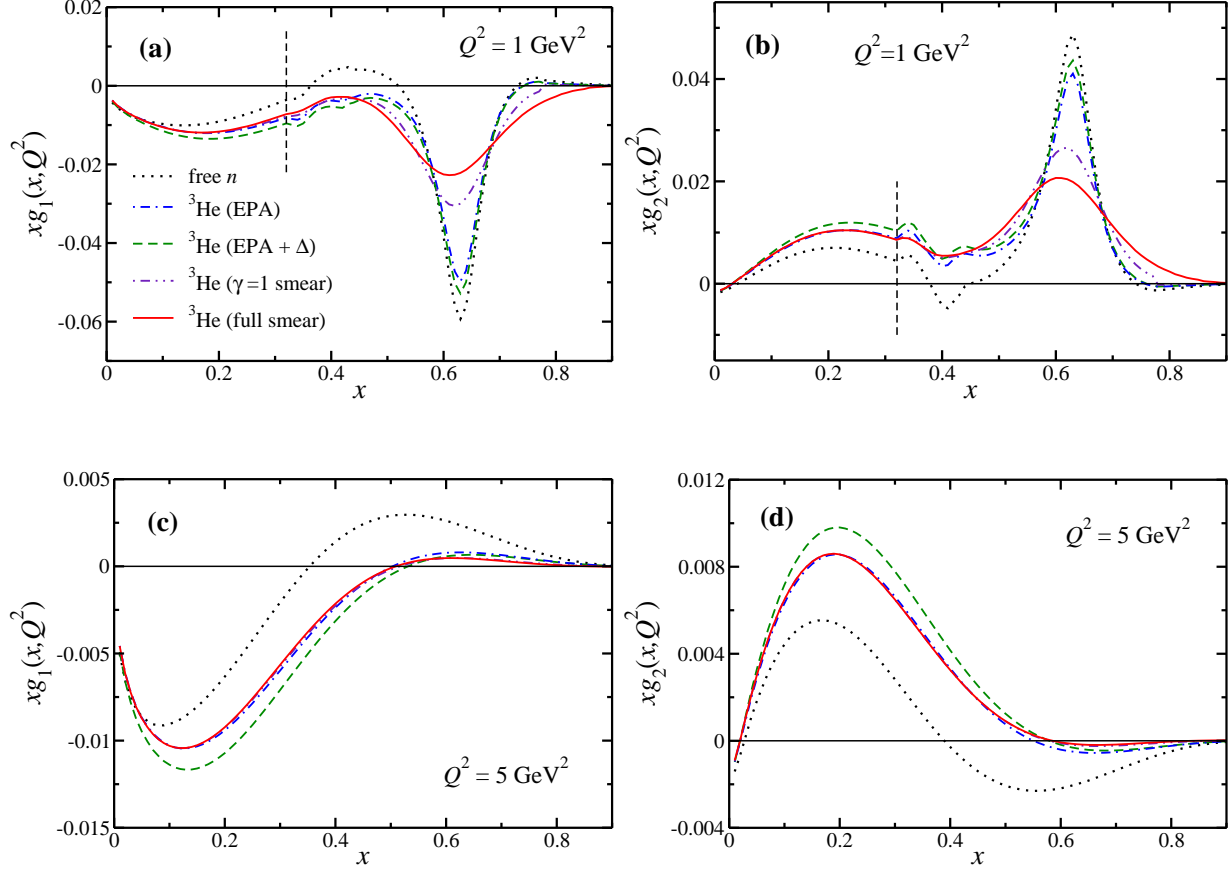


FIG. 2: Spin-dependent  $xg_1$  and  $xg_2$  structure functions of the neutron (black dotted) and  ${}^3\text{He}$ , computed in the EPA with nucleon only (blue dot-dashed) and with  $\Delta$  components (green dashed), and with Fermi smearing in the Bjorken ( $\gamma = 1$ ) limit (violet dot-dot-dashed) and at finite  $Q^2$  (red solid). The functions at  $Q^2 = 1 \text{ GeV}^2$  [(a) and (b)] are computed from the MAID [57] and DSSV [44] parametrizations of the nucleon resonance and DIS regions, respectively (the dashed vertical line indicating the boundary between these), while those at  $Q^2 = 5 \text{ GeV}^2$  [(c) and (d)] use the DSSV fit.

Compared with the free neutron, the  $\Delta$  peak in the  ${}^3\text{He}$  structure functions computed from the full smearing function in Eq. (14) is reduced by more than a factor 2. As noted in Ref. [24] and illustrated in Fig. 2(a) and (b), using the smearing function computed in the Bjorken limit underestimates the amount of smearing, with the  $\Delta$  peak in the  ${}^3\text{He}$  structure function some 20%–30% larger in magnitude than for the full,  $Q^2$ -dependent smearing. The difference between the smeared results and those obtained from the EPA are even more striking, with the EPA reducing the neutron structure functions by only a few percent. The

addition of the  $\Delta$  contribution increases the magnitude of the functions slightly, but in either case it is clear that the approximation of  $x$ -independent nuclear corrections breaks down in the region where the structure is dominated by resonances.

The EPA approach is expected to be more reliable in the DIS region at high  $W$ , where the structure functions are considerably smoother. The corresponding  $xg_1$  and  $xg_2$  functions are illustrated in Fig. 2(c) and (d) at  $Q^2 = 5 \text{ GeV}^2$ . Here the resonance structure at low  $W$  is restricted to larger  $x$ , and for most  $x$  values the functions are dominated by the non-resonant continuum, so that it is reasonable to approximate  $g_1$  and  $g_2$  by the leading twist contributions [44]. Away from the  $x \sim 1$  region, where smearing effects will come into play, one can understand the relative differences between the neutron and  $^3\text{He}$  structure functions simply within the EPA. From Eq. (19) and Table I, the neutron effective polarization  $P_1^n$  reduces the magnitude of the (negative)  $g_1^n$  structure function by  $\approx 15\%$ . However, the proton contribution, which is given by the product of the small (negative) effective polarization,  $2P_1^p \approx -5\%$ , and the large (positive)  $g_1^p$  structure function, shifts the overall  $^3\text{He}$  structure function downward, rendering  $g_1^{^3\text{He}} < g_1^n$ . This is seen in the comparison in Fig. 2(c) and in the DIS region at small  $x$  in Fig. 2(a).

The effects of nuclear smearing in the DIS region, either for  $\gamma = 1$  or including the finite- $Q^2$  corrections, are negligible at  $x \lesssim 0.5$  compared with the EPA with nucleons. At larger  $x$  the smearing effects are more significant, although the magnitude of the structure functions there is considerably smaller. (Note that because the neutron structure function changes sign, it is not practical to consider a ratio of nuclear to nucleon structure functions as in the unpolarized case in Fig. 1.) A larger effect arises with the addition of  $\Delta$  contributions to the  $^3\text{He}$  wave function [15], which accentuates the differences between the free neutron and  $^3\text{He}$  structure functions, especially at intermediate values of  $x$ ,  $0.1 \lesssim x \lesssim 0.4$ . Qualitatively similar behavior is seen for the  $g_2$  structure function in Fig. 2(d), with the signs reversed compared to  $g_1$ . Namely, the neutron polarization slightly reduces the (positive)  $g_2^n$  contribution, while the (negative) proton polarization combines with the (negative)  $g_2^p$  structure function to produce a compensating shift upward, leaving  $g_2^{^3\text{He}} > g_2^n$ . Again, this trend is also seen in the DIS part of the  $g_2$  comparison at  $Q^2 = 1 \text{ GeV}^2$  in Fig. 2(b).

The effects of the (negative)  $\Delta$  resonance contribution to  $g_1^{^3\text{He}}$  are offset somewhat by the nucleon off-shell corrections discussed in Sec. IIID. As illustrated in Fig. 3, the corrections computed within the OCS model give rise to a positive contribution in the intermediate- $x$

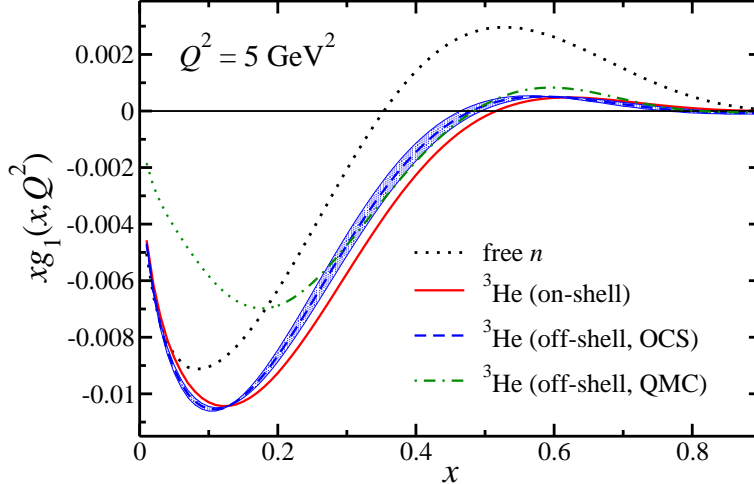


FIG. 3: Nucleon off-shell corrections to the  $xg_1$  structure function of  ${}^3\text{He}$ , within the off-shell covariant spectator model (dashed and shaded band) and in the quark-meson coupling model [46] (dot-dashed) in the valence approximation, with an extrapolation of the latter for  $x \lesssim 0.2$  (light dot-dashed). The free neutron structure function (dotted) and the  ${}^3\text{He}$  structure function computed with on-shell nucleon input (solid) are shown for comparison.

region,  $0.1 \lesssim x \lesssim 0.6$ , where the magnitude of the effects is largest. This will mostly cancel the impact of the  $\Delta$  resonance in this region, bringing the total  ${}^3\text{He}$  structure function closer to the on-shell result. (For simplicity, here we have computed the effects of the smearing in the  $\gamma = 1$  limit, although as Fig. 2 illustrates, at  $Q^2 = 5 \text{ GeV}^2$  the finite- $Q^2$  effects are negligible.) To give an estimate of the uncertainty on this correction, we consider a range of nucleon swelling parameters  $\delta R_N$  between  $\delta R_N/R_N \approx 2\%$  and  $6\%$ , with a central value of  $4\%$ . This gives for the parameter  $\lambda_N$  which determines the  $p^2$  derivative  $\partial g_i^N/\partial p^2$  in Eqs. (34)–(36) the values  $\lambda_n = 0.84 \pm 0.42$  for the neutron and  $\lambda_p = 1.12 \pm 0.56$  for the proton. The corrections corresponding to this range of parameters is indicated in Fig. 3 by the shaded band.

Qualitatively similar behavior is observed using the QMC off-shell model from Steffens *et al.* [46], which gives a small positive shift in  $g_1^{3\text{He}}$  over most of the  $x$  range considered. Note that this model assumes the valence quark approximation, so that its predictions at small  $x$  ( $x \lesssim 0.2$ ) may not be reliable. Nevertheless, it is reassuring that these models, which are based on rather different assumptions, lead to off-shell corrections that are similar in sign and magnitude in their regions of validity.

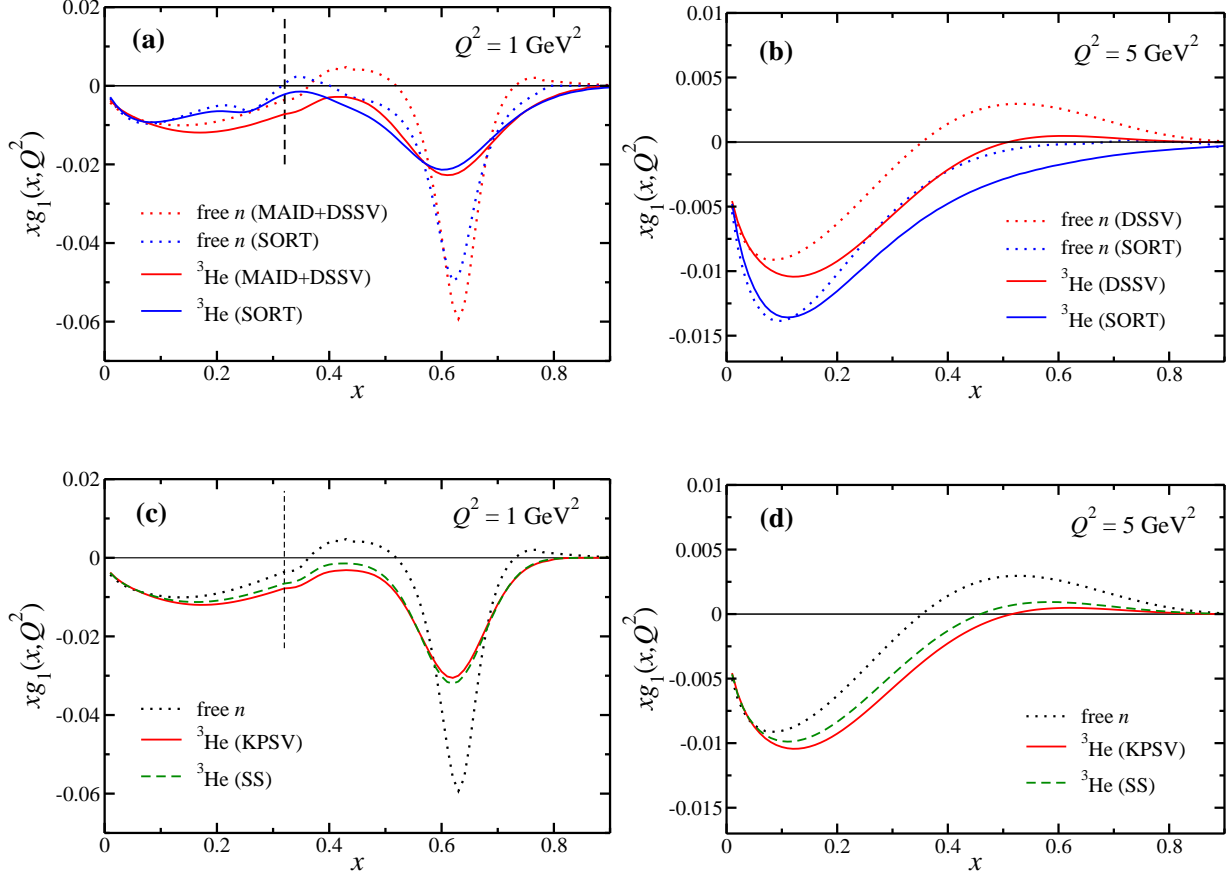


FIG. 4: Dependence of the neutron and  $^3\text{He}$   $g_1$  structure functions on the input nucleon parametrization (MAID [57] and DSSV [44], and SORT [54]) [(a) and (b)], and on the  $^3\text{He}$  wave function (KPSV [12] and SS [11]) [(c) and (d)], at  $Q^2 = 1 \text{ GeV}^2$  and  $5 \text{ GeV}^2$ . The dashed vertical lines at  $Q^2 = 1 \text{ GeV}^2$  indicate the boundary between the nucleon resonance and DIS regions.

While the above results are obtained using specific parametrizations for the input proton and neutron  $g_1$  and  $g_2$  structure functions [44, 57], the detailed predictions for the  $^3\text{He}$  functions will naturally be modified with different nucleon inputs. In Figs. 4(a) and (b) we compare the results for the neutron and  $^3\text{He}$  structure functions, computed using the full smearing functions in Eq. (28), as in Fig. 2, with those using the combined parametrization of the resonance and DIS regions by Simula *et al.* (SORT) [54]. The quantitative differences between the two sets of results reflect the degree to which the structure functions of the free nucleon, and particularly the neutron, are determined experimentally. However, the conclusions about the relative importance of the various nuclear corrections investigated here does not depend on the form of the input distributions. Furthermore, the dependence

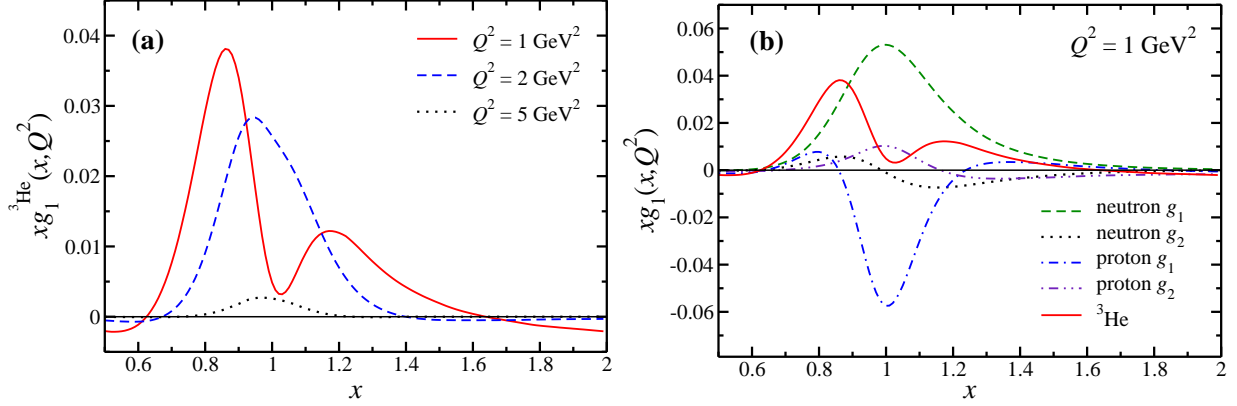


FIG. 5: **(a)** Quasi-elastic contributions to the  $xg_1$  structure function of  ${}^3\text{He}$  at  $Q^2 = 1$  (solid), 2 (dashed) and 5  $\text{GeV}^2$  (dotted). **(b)** Individual contributions to the quasi-elastic  $xg_1$  structure function of  ${}^3\text{He}$  (solid) at  $Q^2 = 1$   $\text{GeV}^2$ , from the neutron  $g_1$  (dashed), neutron  $g_2$  (dotted), proton  $g_1$  (dot-dashed) and proton  $g_2$  (dot-dot-dashed) structure functions.

of the  ${}^3\text{He}$  structure functions on the input neutron  $g_1$  and  $g_2$ , can in principle be removed by applying an iterative procedure, such as that outlined by Kahn *et al.* [58], for example. In practice, the number of iterations required for convergence depends on the number of data points and the precision of the data.

Indeed, the only theoretical input on which the  ${}^3\text{He}$  structure functions in principle depend are the nuclear smearing functions, and whatever approximations are made for them. In Figs. 4(c) and (d) the dependence on the nuclear structure model is illustrated by comparing the  $g_1$  structure function computed from the KPSV [12] and SS [11]  ${}^3\text{He}$  wave functions, at  $Q^2 = 1$   $\text{GeV}^2$  and 5  $\text{GeV}^2$ . To isolate the effects of the wave function alone, the same Bjorken limit ( $\gamma = 1$ ) approximation is used for the smearing functions in the two models. The results in both the resonance region and in the DIS region show a very mild dependence on the wave function, smaller than on the input nucleon structure functions in Figs. 4(a) and (b), suggesting that the theoretical uncertainty arising from the nuclear wave function is not significant.

The dependence on the  ${}^3\text{He}$  wave function model can be reduced by comparing the calculated smearing functions with data on quasi-elastic cross sections. In the impulse approximation these depend simply on the product of the smearing function and the nucleon elastic form factors, Eqs. (10). To the extent that the form factors are determined from data in other elastic or QE scattering reactions, and corrections from final state interactions or

non-nucleonic contributions are not large, measurement of the QE cross sections can directly constrain the smearing function in the vicinity of the QE peak.

The predictions for the QE contribution to the  $g_1$  structure function of  ${}^3\text{He}$  are shown in the WBA in Fig. 5(a) for  $Q^2 = 1, 2$  and  $5 \text{ GeV}^2$ , using the full,  $Q^2$ -dependent smearing functions in Eqs. (14) and (16). For the proton electric and magnetic elastic form factors we use the parametrization from Ref. [59], while the Kelly [60] fit is used for the neutron form factors. As expected, the amplitude of the QE peak fall rapidly with increasing  $Q^2$ , so that by  $Q^2 = 5 \text{ GeV}^2$  the QE contribution is strongly suppressed. At the lowest  $Q^2$  value,  $Q^2 = 1 \text{ GeV}^2$ , the QE contribution exhibits a striking double peak structure, with local maxima at  $x \approx 0.85$  and  $1.2$ , and a dip at  $x \approx 1$ . This is due primarily to the proton  $g_1^p$  contribution, which has a relatively large and negative peak at  $x = 1$ , as Fig. 5(b) illustrates. Although the polarized proton smearing function in  ${}^3\text{He}$  is strongly suppressed relative to the neutron, the larger proton electric form factor  $G_E^p$  compared with the neutron  $G_E^n$  makes the proton and neutron contributions comparable at this  $Q^2$  value.

Future data on inclusive QE cross sections in the  $x \sim 1$  would allow one to investigate this intriguing interplay between the various components of  $g_1^{{}^3\text{He}}$  in detail, and provide a sensitive test of the nuclear wave function. Examination of the tails of the QE cross sections at large  $x$  ( $x \gtrsim 1.6$ ) would also enable exploration of, and possible constraints on, the wave function and nucleon off-shell effects [61].

## B. Asymmetries

While nuclear effects in structure functions have received the greatest attention theoretically, the quantities that are most directly accessible in polarized DIS experiments are the polarization asymmetries  $A_1$  and  $A_2$  in Eqs. (7) (which are themselves extracted from the longitudinal and parallel asymmetries in Eqs. (6)). As ratios of spin-dependent to spin-averaged structure functions, the polarization asymmetries can display more subtle effects arising from the  $x$  dependence of the polarized  $g_{1,2}$  and unpolarized  $F_{1,2}$  structure functions, and the nuclear corrections to these, especially in the resonance nucleon region.

In Fig. 6 the  $A_1$  and  $A_2$  asymmetries of the neutron and  ${}^3\text{He}$  are shown at  $Q^2 = 1$  and  $5 \text{ GeV}^2$  for the various nuclear models considered in Fig. 2. Note that since  $g_{1,2}^{{}^3\text{He}} \approx g_{1,2}^n$ , while  $F_1^{{}^3\text{He}} \gg F_1^n$ , the absolute value of the  ${}^3\text{He}$  asymmetry will be considerably smaller than that



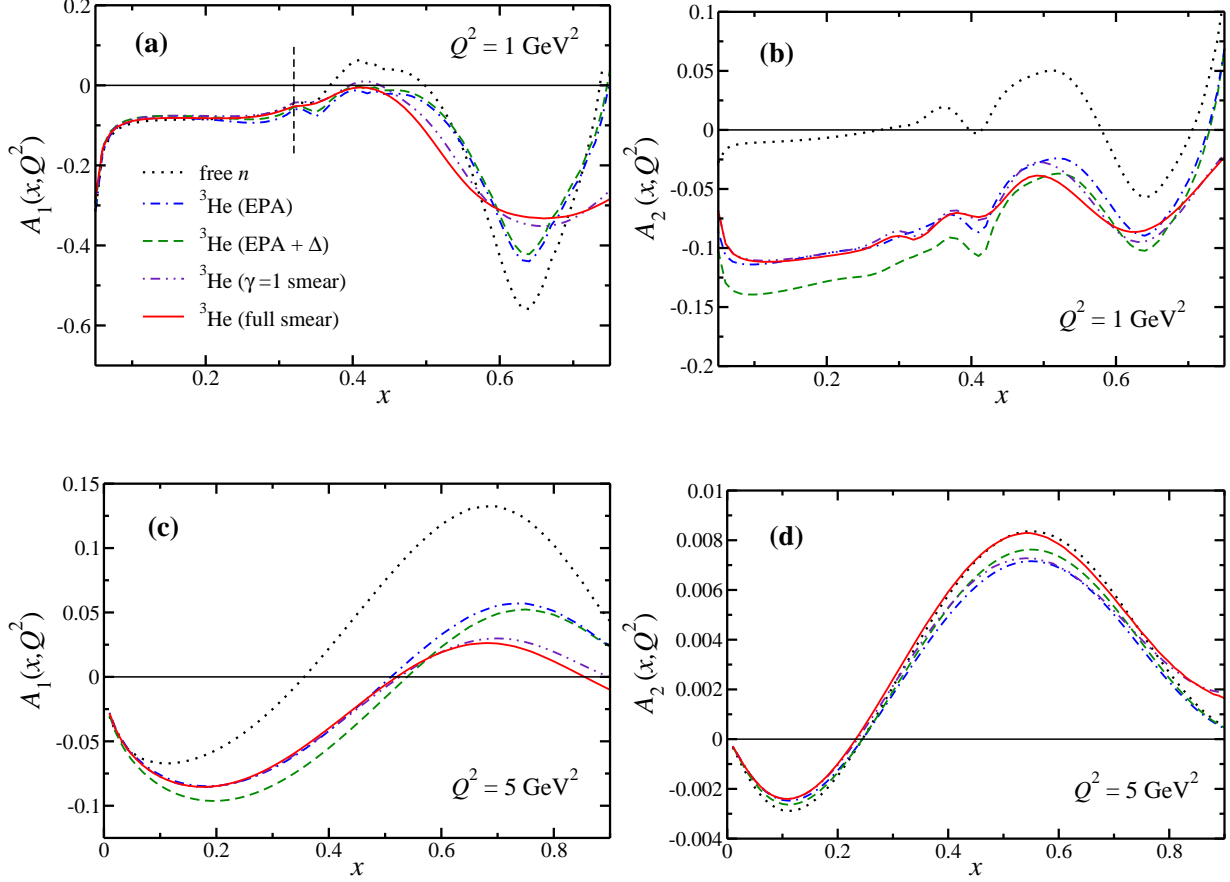


FIG. 6: As in Fig. 2, but for the polarization asymmetries  $A_1$  and  $A_2$  of the neutron and  ${}^3\text{He}$  at  $Q^2 = 1 \text{ GeV}^2$  [(a) and (b)] and  $Q^2 = 5 \text{ GeV}^2$  [(c) and (d)], constructed from ratios of the spin-dependent structure functions in Fig. 2 and the unpolarized  $F_1$  structure function from the Bosted-Christy parametrization [55]. Note that the  ${}^3\text{He}$  asymmetries are scaled by a factor  $(1 + 2F_1^p/F_1^n)$ .

of the neutron asymmetry. To display both the neutron and  ${}^3\text{He}$  asymmetry results on the same scale, we multiply the latter by the factor  $(1 + 2F_1^p/F_1^n)$ , which compensates for the suppression of  $A_{1,2}^{3\text{He}}$  due to the small proton contribution to  $g_{1,2}^{3\text{He}}$ ,

$$A_1^{3\text{He}} = \frac{(g_1^{3\text{He}} - (\gamma^2 - 1)g_2^{3\text{He}})}{F_1^{3\text{He}}} \longrightarrow A_1^{3\text{He}} \times \left(1 + \frac{2F_1^p}{F_1^n}\right), \quad (41a)$$

$$A_2^{3\text{He}} = \sqrt{\gamma^2 - 1} \frac{(g_1^{3\text{He}} + g_2^{3\text{He}})}{F_1^{3\text{He}}} \longrightarrow A_2^{3\text{He}} \times \left(1 + \frac{2F_1^p}{F_1^n}\right). \quad (41b)$$

For the  $A_1$  asymmetry, the effect of the nuclear corrections is qualitatively similar to that for the  $g_1$  structure function in Fig. 2. The nuclear smearing corrections have the largest

impact in the nucleon resonance region, particularly in the vicinity of the  $\Delta$  resonance, although the magnitude of the effect is slightly smaller compared to that for  $g_1$ . Since both the numerator and denominator in the  $^3\text{He}$  asymmetry involve smeared structure functions, the relative effects of the smearing on  $A_1^{^3\text{He}}$  will be reduced. Note that for the isovector  $\Delta$  resonance, the scaling factor in Eqs. (41) is  $1 + 2F_1^p/F_1^n \approx 3$ . At larger  $x$ , in the region  $W \lesssim M_\Delta$ , the free neutron asymmetry computed from the MAID parametrization of  $g_1$  and  $g_2$  rises steeply, which suggests that the  $F_1^n$  denominator from the Bosted-Christy fit falls rapidly in this region. A similar trend is observed when using the SORT parametrization [54] of the spin-dependent structure functions. The general features of the  $A_1$  asymmetry in the DIS region at  $Q^2 = 5 \text{ GeV}^2$  are similar to those of the  $g_1$  structure function in Fig. 2(c). Namely, with the rescaling factor in Eqs. (41), the asymmetries at  $x \ll 1$  are basically given by the corresponding  $g_1$  structure functions divided by the  $F_1^n$  structure function, with the scaled  $^3\text{He}$  asymmetry below the free neutron asymmetry.

For the  $A_2$  asymmetry, which is proportional to the sum of the  $g_1$  and  $g_2$  structure functions, the resulting scaled  $^3\text{He}$  asymmetry at  $Q^2 = 5 \text{ GeV}^2$  is very similar to the input  $A_2^n$ . Here, the dominant leading twist contribution to  $A_2$  is given by the integral term  $\int (dz/z)g_1(z)$  on the right-hand-side of Eq. (12). Therefore, the differences between the  $A_2$  asymmetries of the neutron and  $^3\text{He}$  at leading twist will be determined by the nuclear effects on the  $g_1$  structure function. As is evident from Figs. 2(c) and (d), the nuclear corrections lower the  $^3\text{He}$  structure function relative to the neutron for  $g_1$  but raise it for  $g_2$ , the net effect of which is a strong cancellation of the nuclear effects (for both the EPA and smearing calculations) which leaves  $A_2^n \approx A_2^{^3\text{He}}(1 + 2F_1^p/F_1^n)$  at  $x \ll 1$ . The cancellations are not as evident at the lower,  $Q^2 = 1 \text{ GeV}^2$  value, where the resonance structures dominate and the WW approximation (12) to  $g_2$  is in general not valid. Here the prominent  $\Delta$  resonance peaks in  $g_1$  (negative) and  $g_2$  (positive) in Fig. 2 largely cancel, resulting in a  $^3\text{He}$   $A_2$  asymmetry that is several times smaller than the corresponding  $A_1$  asymmetry at the  $\Delta$  peak in Fig. 6(a). Because of the  $\sqrt{\gamma^2 - 1}$  factor in the definition of  $A_2$  in Eq. (7b), the overall magnitude of the  $A_2$  asymmetry at lower  $Q^2$  (larger  $\gamma$ ) is almost an order of magnitude larger than that at  $Q^2 = 5 \text{ GeV}^2$  in Fig. 6(d).

From simple counting rule and perturbative QCD arguments, in the  $x \rightarrow 1$  limit DIS from quarks with spins aligned with the spin of the nucleon is expected to dominate over scattering from quarks with spins antialigned [62–66]. At leading twist, the proton and

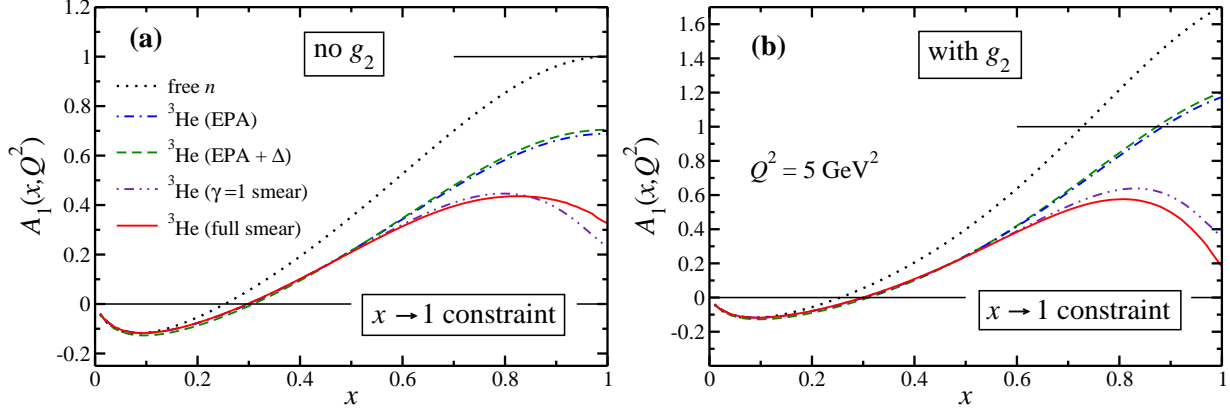


FIG. 7: Polarization asymmetry  $A_1$  of the neutron and  ${}^3\text{He}$  computed using the input LSS [67] parametrization constrained by  $A_1 \rightarrow 1$  as  $x \rightarrow 1$ . The asymmetries are computed (a) with  $g_1$  contributions only and (b) including also  $g_2$  corrections in Eq. (7a), which push the  $A_1$  asymmetry above unity at large  $x$  at  $Q^2 = 5 \text{ GeV}^2$ . The nuclear models are as in Fig. 6, and the the  ${}^3\text{He}$  asymmetry is scaled by a factor  $(1 + 2F_1^p/F_1^n)$ .

neutron polarization asymmetries should therefore approach unity,  $A_1 \rightarrow 1$  as  $x \rightarrow 1$ . A number of other, nonperturbative models also make specific predictions for the large- $x$  behavior of  $A_1^n$ , making this quantity particularly sensitive to the dynamics of valence quarks in the nucleon. Because of the lack of data on spin structure functions or asymmetries at very large  $x$ , however, the  $x \rightarrow 1$  behavior is usually not addressed in standard PDF parametrizations, such as the DSSV fit [44] used in Fig. 6, and the behavior at  $x \gtrsim 0.8$  is left unconstrained. To illustrate the possible effects of the perturbative  $x \rightarrow 1$  expectations on the spin-dependent PDFs, Leader, Sidorov and Stamenov [67] performed a global fit with polarized and unpolarized PDFs constrained with  $\Delta q/q \rightarrow 1$  as  $x \rightarrow 1$  [66], which at large  $Q^2$  forces  $A_1 \rightarrow g_1/F_1 \rightarrow 1$ . The neutron asymmetry with this constraint is illustrated in Fig. 7(a), where for simplicity the  $g_2$  contribution is omitted.

The question we would like to address in this work is how the nuclear corrections in  ${}^3\text{He}$  would affect such behavior, and the degree to which these corrections can be reliably subtracted to reveal the true dependence of  $A_1^n$  on  $x$  as  $x \rightarrow 1$ . Within the EPA, the  ${}^3\text{He}$  asymmetry is reduced by  $\approx 30\%$  in the  $x \rightarrow 1$  limit relative to the neutron asymmetry, for the same reasons that the effective polarizations render  $g_1^{3\text{He}} < g_1^n$  in Fig. 2(c), for example, and that the scaled  ${}^3\text{He}$  asymmetry lies below  $A_1^n$  in Fig. 6(c) for the DSSV parametrization. The effect of the nuclear smearing is a further reduction of  $A_1^{3\text{He}}$  to  $\approx 0.25 - 0.35$  at  $Q^2 =$

5 GeV<sup>2</sup>, depending on whether the full,  $Q^2$ -dependent smearing function is used or its  $\gamma = 1$  approximation. Including the  $g_2$  terms in Eq. (7a), the free neutron  $A_1$  asymmetry, computed from the LSS parametrization [67] using the WW relation (12) for  $g_2^n$ , increases by  $\gtrsim 60\%$  at  $x \approx 1$  for  $Q^2 = 5$  GeV<sup>2</sup>, as Fig. 7(b) illustrates. (Recall from Fig. 2(d) that the twist-2 part of  $g_2^n$  is negative at large  $x$ .) The resulting <sup>3</sup>He asymmetries are correspondingly larger, although the effects of the  $Q^2$ -dependent smearing are even more pronounced in the presence of the  $g_2$  contributions. With the upcoming high-precision experiments to determine the  $x \rightarrow 1$  behavior of  $A_1^n$  from measurements of the <sup>3</sup>He polarization asymmetries planned at Jefferson Lab at 12 GeV [68, 69], it will therefore be crucial to account for the finite- $Q^2$  and nuclear smearing corrections in the large- $x$  region.

### C. Moments

The nuclear corrections examined in this analysis clearly have a significant impact on the shape of the structure functions, especially at large values of  $x$ . Since in this region the structure functions themselves are typically small, one may expect that the nuclear effects on integrals of structure functions, or moments  $\Gamma_i^{(n)}$ , may be reduced. This would be expected particularly of the low moments, which are most sensitive to the small- $x$  region, whereas higher moments progressively emphasize the large- $x$  tails of distributions with increasing rank  $n$ .

In QCD, the moments of structure functions are formally related through the operator product expansion to hadronic matrix elements of local operators of a given twist, and can be directly computed from first principles in lattice QCD or approximated in low-energy model calculations. Various sum rules, such as the Bjorken [41], Gerasimov-Drell-Hearn [70] or Burkhardt-Cottingham [30] sum rules, can then provide important tests of QCD and its applications to nucleon structure. Sum rules involving moments of neutron structure functions (for example, the Bjorken sum rule, which relates the isovector combination  $g_1^p - g_1^n$  to the axial charge,  $g_A$ ) require the nuclear corrections to be known to a sufficient level of accuracy.

The effect of the nuclear corrections on the neutron  $\Gamma_1^{(n)}$  and  $\Gamma_2^{(n)}$  moments are illustrated in Fig. 8 for the  $n = 1$  and  $n = 5$  moments from  $Q^2 = 1$  to 5 GeV<sup>2</sup>. For the  $g_1$  moments the DSSV [44] and MAID [57] parametrizations are used for the proton and neutron structure

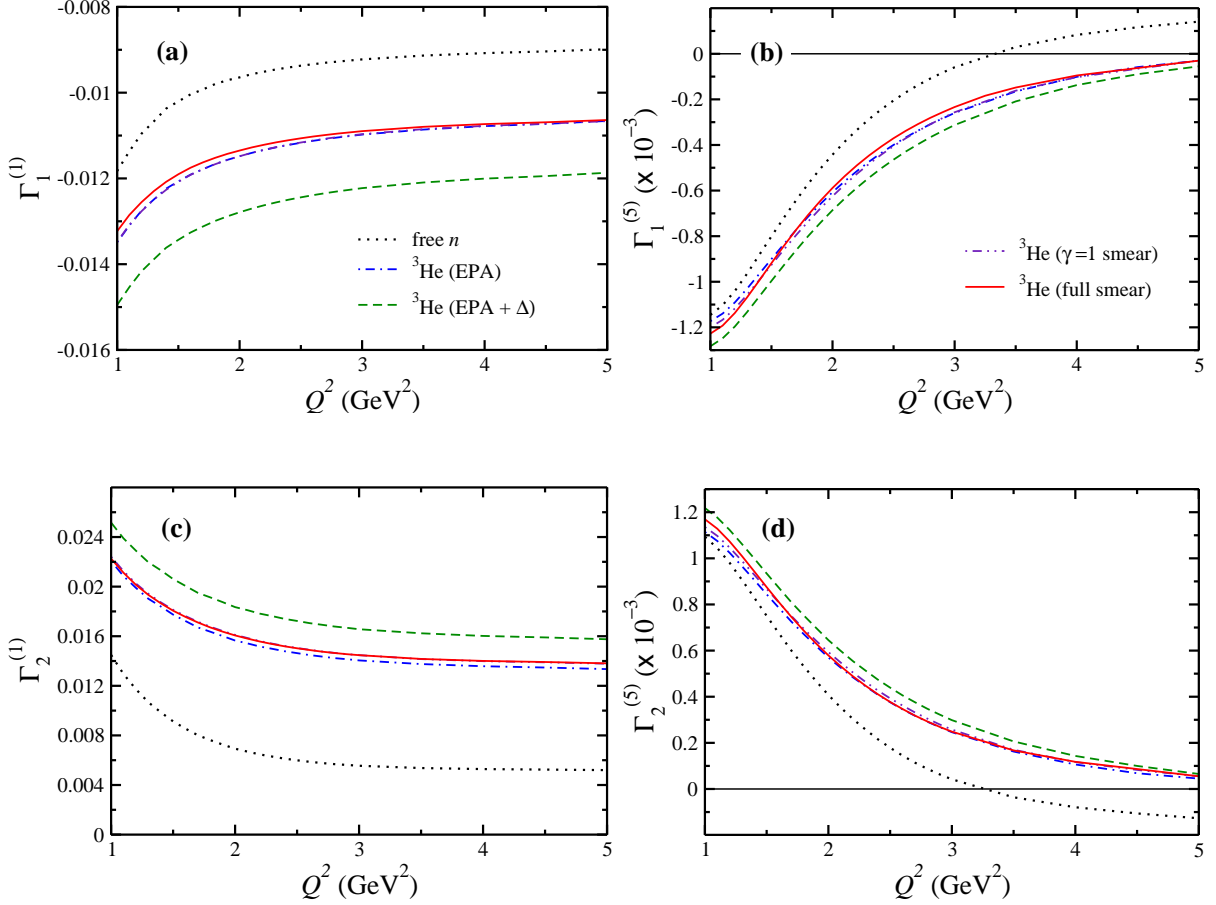


FIG. 8: Moments of the neutron and  $^3\text{He}$   $g_1$  structure functions,  $\Gamma_1^{(n)}$  [(a) and (b)] and of the corresponding  $g_2$  structure functions,  $\Gamma_2^{(n)}$  [(c) and (d)], for  $n = 1$  and  $n = 5$ . The  $^3\text{He}$  moments are computed in the EPA with nucleons only (dot-dashed) and with  $\Delta$  components (dashed), and with Fermi smearing for  $\gamma = 1$  (dot-dot-dashed) and at finite  $Q^2$  (solid). The  $g_1$  moments are computed from the DSSV [44] and MAID [57] parametrizations of the proton and neutron structure functions in the DIS and resonance regions, respectively, while the  $g_2$  moments assume the WW relation (12) for the DIS region and the MAID fit for the resonance part.

functions in the DIS and resonance regions, respectively, while the  $g_2$  moments assume the WW relation (12) for the DIS region and the MAID fit for the resonance component. For the lowest,  $n = 1$  moment computed within the EPA with nucleon contributions only, the neutron effective polarization  $P_1^n$  reduces the magnitude of the (negative) neutron moment by  $\sim 15\%$ . However, while the total proton polarization is small,  $2P_1^p \sim -5\%$ , the much larger value of the (positive) proton moment  $\Gamma_1^{p(1)}$  more than compensates, rendering the overall correction to the  $^3\text{He}$  moment negative ( $\sim 20\%$  larger magnitude). Because the

lowest moment is dominated by the small- $x$  contributions, the effects of nuclear smearing are negligible, with only small differences visible between the full,  $Q^2$ -dependent smearing and that in the Bjorken ( $\gamma = 1$ ) limit. More important is the contribution from the  $\Delta$  resonance, which is assumed in the EPA calculation of Sec. III C to be present at all  $x$ . This gives a negative contribution to the  ${}^3\text{He}$  moment which is comparable in magnitude to that from the effective nucleon polarization correction.

Small- $x$  contributions are suppressed for higher moments, as seen in Fig. 8(b) for the  $n = 5$  moment of  $g_1$ . In this case the relative effect of the nuclear smearing is enhanced, although not significantly, while the effect of the  $\Delta$  resonance correction is reduced compared with the lowest moment. Note that because of the suppression of the small- $x$  region by the factor  $x^4$  in Eq. (9), the magnitude of the  $\Gamma_1^{(5)}$  moment is smaller by at least an order of magnitude compared with  $\Gamma_1^{(1)}$ .

The behavior of the  $g_2$  moments in Figs. 8(c) and (d) is qualitatively similar to the  $g_1$  moments. Generally the sign of the  $g_2$  structure function and its moments are opposite from that of  $g_1$ , but the overall effects of the various approximations for the nuclear corrections are analogous. Namely, the EPA raises the magnitude of  $\Gamma_2^{(n)}$  for  ${}^3\text{He}$  from the neutron value due to the overall positive proton contribution (since the proton  $\Gamma_2^{(n)}$  is negative), with the  $\Delta$  resonance contribution giving an additional small increase. The effect of the latter is reduced for the  $n = 5$  moment, and the effects of the smearing are again relatively small. Note that the smearing effects preserve the vanishing of the lowest ( $n = 1$ ) moment of  $g_2$ ,  $\Gamma_2^{3\text{He}(1)}\Big|_{\text{WW}} = 0$ , so that the nonzero values of  $\Gamma_2^{(1)}$  in Fig. 8(c) are entirely due to the resonance contributions, which need not satisfy the WW relation.

Since the moments of structure functions are formally defined as integrals over the entire range of  $x$  between 0 and 1, they in principle contain contributions from elastic scattering at  $x = 1$  for the nucleon, and from QE scattering at  $x \approx 1$  for  ${}^3\text{He}$ . The elastic and QE contributions are strongly suppressed with increasing  $Q^2$ , but can be significant at  $Q^2 = \mathcal{O}(1 \text{ GeV}^2)$ , as Fig. 9 illustrates for the  $\Gamma_1^{(1)}$  and  $\Gamma_1^{(5)}$  moments. As in Fig. 5, the electromagnetic form factors of the proton are taken from the parametrization of Ref. [59], and the neutron form factors from Ref. [60], although the dependence on the form factor fit is small. For higher moments, the magnitude of the inelastic contributions (at  $x < 1$ ) is suppressed by the factor  $x^n$ , whereas the elastic contribution (at  $x = 1$ ) remains the same for all moments. The QE contribution to the  $\Gamma_1^{(5)}$  moment is therefore significantly larger

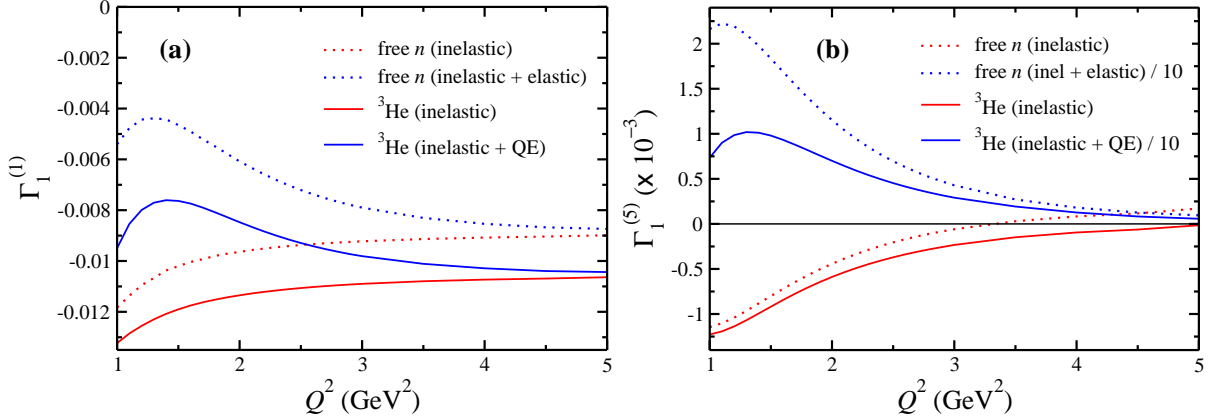


FIG. 9: Contributions from elastic and quasi-elastic scattering to the neutron and  ${}^3\text{He}$   $g_1$  moments, for (a)  $\Gamma_1^{(1)}$  and (b)  $\Gamma_1^{(5)}$ , compared with the inelastic contributions. The elastic and QE components are scaled by a factor 1/10 for clarity.

than the inelastic, especially at low  $Q^2$  values, and for clarity in Fig. 9(b) the sum of the inelastic and elastic (or QE) is scaled by a factor 1/10.

Finally, to estimate the nuclear corrections to the  $d_2$  moment of the neutron defined in Eq. (11), in Fig. 10 we show the  $d_2$  moments for  ${}^3\text{He}$  computed using the various approximations for the nuclear effects discussed above. The  $d_2$  moment is of interest because of its unique sensitivity to higher twist contributions to the  $g_2$  structure function (the leading twist contribution from the WW relation vanishes, as seen from Eqs. (11) and (12)). The  $d_2$  moment of the  ${}^3\text{He}$  structure functions was recently measured at Jefferson Lab in the E06-014 experiment [28]. The data are currently being analyzed, and are expected to have a statistical precision of  $\pm 0.4 \times 10^{-3}$  over the  $Q^2$  range between 2 and 5  $\text{GeV}^2$ , with an average  $\langle Q^2 \rangle \approx 4 \text{ GeV}^2$  [71].

Using the MAID and DSSV parametrizations for  $g_1$  and  $g_2$  for the nucleon resonance and DIS regions, respectively, as in Fig. 2 for instance, only the former makes a nonzero contribution to the  $d_2$  moment (the DSSV fit is performed exclusively in terms of leading twist PDFs). The MAID resonance fit gives rise to  $d_2$  values which drop precipitously with  $Q^2$ . The nuclear corrections to  $d_2$  are small in absolute terms, but increase dramatically with  $Q^2$  for the ratio  $d_2^{3\text{He}}/d_2^n$  for all the models considered, such that  $d_2^{3\text{He}}$  is  $\approx 2$  times larger than  $d_2^n$  at  $Q^2 \approx 3 \text{ GeV}^2$ , and  $\approx 4$  times larger at  $Q^2 \approx 4 \text{ GeV}^2$ . The effect of the nuclear smearing is minimal compared with the EPA, although the possible  $\Delta$  resonance

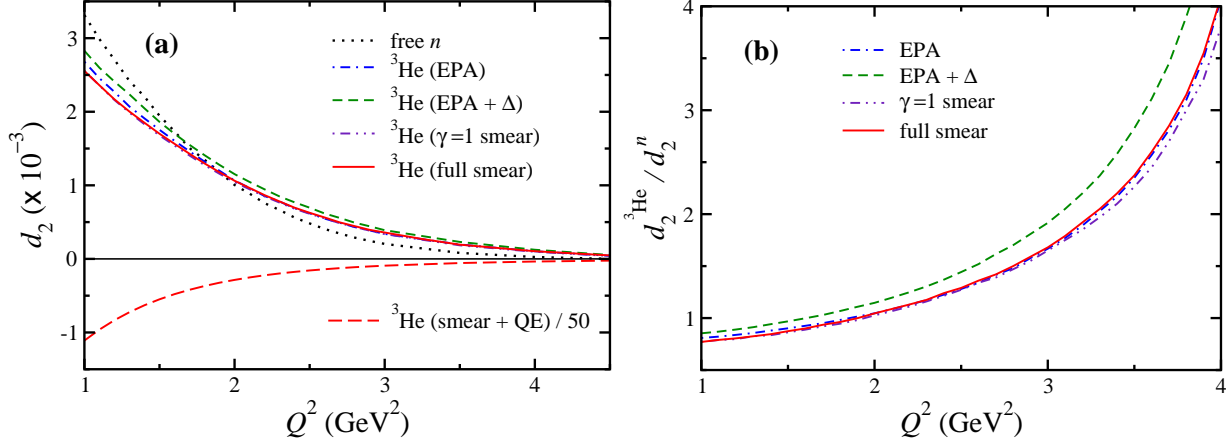


FIG. 10: **(a)**  $d_2$  moment of the neutron (dotted) and  $^3\text{He}$ , with the latter computed in the EPA with nucleons only (dot-dashed) and with  $\Delta$  components (dashed), and with Fermi smearing for  $\gamma = 1$  (dot-dot-dashed) and the full smearing at finite  $Q^2$  (solid). The  $d_2$  moment for  $^3\text{He}$  including the QE contribution (scaled by a factor  $1/50$ ) is shown for comparison (long-dashed). **(b)** Ratio of the  $d_2$  moments for  $^3\text{He}$  and the neutron, with the  $^3\text{He}$  moments computed using the various approximations in (a).

component of the  $^3\text{He}$  wave functions makes a non-negligible contribution to the ratio in Fig. 10(b). Nucleon off-shell effects may also give rise to corrections to  $d_2^n$ , however, these are difficult to estimate using the (leading twist) quark models discussed in Sec. III D. At low  $Q^2$ , the QE contribution in Fig. 10(a) is significantly larger than the inelastic, and remains sizeable at larger  $Q^2$  also. Accurate extraction of  $d_2^n$  from the  $^3\text{He}$  data will therefore require precise knowledge of the nuclear effects and the elastic nucleon form factors over the  $Q^2$  range considered here.

## V. CONCLUSION

For the foreseeable future, polarized  $^3\text{He}$  targets will remain an essential tool for studying the spin structure of the nucleon, providing the most direct means of probing the spin-dependent quark and gluon distribution in the free neutron. With the ever increasing levels of precision attained in new generations of polarized DIS experiments, including in previously unexplored regions of kinematics, comes the need for correspondingly better understanding of the nuclear effects that differentiate between the structure of the free neutron and that



bound in the  ${}^3\text{He}$  nucleus.

In this paper we have performed a comprehensive analysis of nuclear corrections to the spin-dependent  $g_1$  and  $g_2$  structure functions and their moments, as well as the  $A_1$  and  $A_2$  polarization asymmetries which are also sensitive to nuclear effects in unpolarized  ${}^3\text{He}$  structure functions. We have contrasted various methods of accounting for the nuclear corrections, including through the use of effective polarizations, and nuclear smearing functions computed in the framework of the weak binding approximation. Generally, the effective polarization approximation does not provide a reliable means of describing the differences between the  ${}^3\text{He}$  and neutron structure functions, especially in the low- $W$  region dominated by nucleon resonances and in the DIS region at large values of  $x$ . In these regions in particular it is important to treat the  $Q^2$  dependence in the smearing functions correctly, as the comparison with the smearing computed in the Bjorken ( $\gamma = 1$ ) limit illustrates that the latter significantly underestimates the strength of the effect. On the other hand, at intermediate  $x$  values and at  $W$  above the resonance region, where the structure functions are smooth and slowly varying, nuclear smearing provides only a relatively minor improvement over the EPA approach.

In addition to the corrections arising from the incoherent nucleon impulse approximation, we have also examined contributions from non-nucleonic degrees of freedom in the nucleus, specifically the  $\Delta$  resonance. Following Bissey *et al.* [13], we relate the strength of this correction to the Bjorken sum rule in  $A = 3$  nuclei, and confirm sizeable contributions at small and intermediate values of  $x$ , which consequently have greatest impact on the lowest moments of the  $g_1$  and  $g_2$  structure functions. Corrections associated with the nucleon off-shell structure have also been estimated in a covariant spectator model, with the magnitude determined by the change in the size of the nucleon radius in the  ${}^3\text{He}$  nucleus, as well as from a quark-meson coupling model. In both cases the off-shell corrections were found to cancel somewhat the effects of the  $\Delta$  contribution, although these corrections at present are difficult to quantify model-independently.

Our analysis complements earlier studies of nuclear corrections to spin-dependent structure functions, where some of these effects were partially explored. It also provides estimates of the nuclear corrections to the  $d_2$  moment of the neutron, measured recently in the E06-014 experiment at Jefferson Lab [28], which offers a direct window on the higher twist component of the  $g_2$  structure function. The QE contribution to the  $d_2$  moment of  ${}^3\text{He}$  is found to

be significant, requiring this component to be determined to a high level of accuracy when extracting the neutron  $d_2$  results.

Measurement of the QE contributions to the polarized inclusive  $^3\text{He}$  cross sections can in future provide an important test of the nucleon smearing functions in  $^3\text{He}$ . We have found non-trivial cancellations between QE proton and neutron contributions to the  $g_1$  structure function of  $^3\text{He}$ , which is particularly striking at intermediate values of  $Q^2 \sim 1 \text{ GeV}^2$ .

While the goal of many  $^3\text{He}$  DIS experiments is ultimately the extraction of information on the structure of the free neutron, this is relatively straightforward only for moments of the structure functions. Our calculations of the nuclear corrections should provide a reliable estimate of the size of these corrections and their uncertainties. Extraction of the neutron polarization asymmetries  $A_{1,2}^n$  and structure functions  $g_{1,2}^n$  is more challenging, on the other hand, especially in the nucleon resonance region. Here this will require unfolding the neutron structure information by making use of a deconvolution procedure, stepping through several iterations until convergence is achieved. As found by Kahn *et al.* [58], typically this involves just a handful of iterations, depending on the level of accuracy required in the reconstruction, although precision data are needed to obtain errors comparable to those for the free proton [72].

Definitive tests of the nuclear correction methods would be possible through independent determination of the free neutron structure in experiments where the nuclear effects are minimal or absent altogether [73]. Examples of such processes include the polarized version of the MARATHON proposal [74] at Jefferson Lab, which will measure the ratio of inclusive  $^3\text{He}$  to  $^3\text{H}$  structure functions, from which the  $d$  to  $u$  quark PDF ratio will be extracted. For unpolarized scattering, nuclear corrections were found [75] to cancel to within  $\approx 1\%$  up to  $x \approx 0.85$ , and similar effect are expected for the spin-dependent case. An alternative approach would be to perform semi-inclusive DIS from polarized  $^3\text{He}$ , with detection of correlated  $pp$  pairs that would indicate scattering from the bound neutron. Detection of such pairs with low momentum at backward angles would minimize the degree to which the struck neutron was off shell and eliminate contamination from final state interactions, in analogy with the BONuS experiment at Jefferson Lab with an unpolarized deuteron target [76]. A more challenging method that would be completely free of nuclear contamination would be parity-violating DIS of unpolarized leptons from polarized protons [77, 78]. The polarization asymmetry here would be sensitive to the spin-dependent  $\gamma Z$  interference structure func-

tions, thus providing an independent combination of the polarized  $\Delta u$  and  $\Delta d$  PDFs at large  $x$  from which the free neutron structure function could be unambiguously reconstructed.

### Acknowledgments

We thank S. Kulagin for helpful discussions about nuclear effects in  $^3\text{He}$ , L. Brady for assistance with the nucleon off-shell corrections, and D. Parno for discussions about the E06-014 data. This work was supported by the U.S. Department of Energy contract No. DE-AC05-06OR23177, under which Jefferson Science Associates, LLC operates Jefferson Lab. J.E. was partially supported by the SULI program of the DOE, Office of Science.

- 
- [1] J. P. Chen, A. Deur, S. Kuhn and Z.-E. Meziani, *J. Phys. Conf. Ser.* **299**, 012005 (2011).
  - [2] C. A. Aidala, S. D. Bass, D. Hasch and G. K. Mallot, *Rev. Mod. Phys.* **85**, 655 (2013).
  - [3] L. Frankfurt and M. Strikman, *Nucl. Phys.* **A405**, 557 (1983).
  - [4] B. Blankleider and R. M. Woloshyn, *Phys. Rev. C* **29**, 538 (1984).
  - [5] R. M. Woloshyn, *Nucl. Phys.* **A496**, 749 (1989).
  - [6] C. Ciofi degli Atti, E. Pace and G. Salmè, *Phys. Rev. C* **46**, R1591 (1992).
  - [7] C. Ciofi degli Atti, S. Scopetta, E. Pace and G. Salmè, *Phys. Rev. C* **48**, R968 (1993).
  - [8] C. Ciofi degli Atti, E. Pace and G. Salmè, *Phys. Rev. C* **51**, 1108 (1995).
  - [9] C. Ciofi degli Atti and S. Scopetta, *Phys. Lett. B* **404**, 223 (1997).
  - [10] L. P. Kaptari and A. Yu. Umnikov, *Phys. Lett. B* **240**, 203 (1990).
  - [11] R.-W. Schulze and P. U. Sauer, *Phys. Rev. C* **48**, 38 (1993).
  - [12] A. Kievsky, E. Pace, G. Salmè and M. Viviani, *Phys. Rev. C* **56**, 64 (1997).
  - [13] F. R. P. Bissey, A. W. Thomas and I. R. Afnan, *Phys. Rev. C* **64**, 024004 (2001).
  - [14] C. Boros, V. A. Guzey, M. Strikman and A. W. Thomas, *Phys. Rev. D* **64**, 014025 (2001).
  - [15] F. R. P. Bissey, V. A. Guzey, M. Strikman and A. W. Thomas, *Phys. Rev. C* **65**, 064317 (2002).
  - [16] S. Scopetta, *Phys. Rev. C* **70**, 015205 (2004).
  - [17] S. Scopetta, *Phys. Rev. D* **75**, 054005 (2007).
  - [18] W. Melnitchouk, G. Piller and A. W. Thomas, *Phys. Lett. B* **346**, 165 (1995).

- [19] G. Piller, W. Melnitchouk and A. W. Thomas, Phys. Rev. C **54**, 894 (1996).
- [20] R.-W. Schulze and P. U. Sauer, Phys. Rev. C **56**, 2293 (1997).
- [21] S. A. Kulagin, G. Piller and W. Weise, Phys. Rev. C **50**, 1154 (1994).
- [22] S. A. Kulagin, W. Melnitchouk, G. Piller and W. Weise, Phys. Rev. C **52**, 932 (1995).
- [23] S. A. Kulagin and W. Melnitchouk, Phys. Rev. C **77**, 015210 (2008).
- [24] S. A. Kulagin and W. Melnitchouk, Phys. Rev. C **78**, 065203 (2008).
- [25] L. Frankfurt, V. Guzey and M. Strikman, Phys. Lett. B **381**, 379 (1996).
- [26] V. Guzey and M. Strikman, Phys. Rev. C **61**, 014002 (2000).
- [27] B. Budick, J. S. Chen and H. Lin, Phys. Rev. Lett. **67**, 2630 (1991).
- [28] Jefferson Lab experiments E06-014, S. Choi, X. Jiang, Z.-E. Meziani and B. Sawatzky spokespersons.
- [29] S. Wandzura and F. Wilczek, Phys. Lett. B **72**, 195 (1977).
- [30] H. Burkhardt and W. N. Cottingham, Ann. Phys. **56**, 453 (1970).
- [31] G. Piller and W. Weise, Phys. Rep. **330**, 1 (2000).
- [32] S. A. Kulagin and R. Petti, Nucl. Phys. **A765**, 126 (2006).
- [33] J. L. Friar *et al.*, Phys. Rev. C **42**, 2310 (1990).
- [34] A. Stadler, P. U. Sauer and W. Glöckle, Phys. Rev. C **44**, 2319 (1991).
- [35] M. Ericson and A. W. Thomas, Phys. Lett. B **128**, 112 (1983).
- [36] L. P. Kaptari, A. I. Titov, E. L. Bratkovskaya and A. Yu. Umnikov, Nucl. Phys. **A512**, 684 (1990).
- [37] L. P. Kaptari and A. Yu. Umnikov, Phys. Lett. B **272**, 359 (1991).
- [38] W. Melnitchouk and A. W. Thomas, Phys. Rev. D **47**, 3783 (1993).
- [39] I. C. Cloët, W. Bentz and A. W. Thomas, Phys. Rev. Lett. **102**, 252301 (2009).
- [40] T.-Y. Saito, Y. Wu, S. Ishikawa and T. Sasakawa, Phys. Lett. B **242**, 12 (1990).
- [41] J. D. Bjorken, Phys. Rev. **148**, 1467 (1966).
- [42] F. E. Close and A. W. Thomas, Phys. Lett. B **212**, 227 (1988).
- [43] C. Boros and A. W. Thomas, Phys. Rev. D **60**, 074017 (1999).
- [44] D. de Florian, R. Sassot, M. Stratmann and W. Vogelsang, Phys. Rev. D **80**, 034030 (2009).
- [45] M. Glück, E. Reya, M. Stratmann and W. Wogelsang, Phys. Rev. D **63**, 094005 (2001).
- [46] F. M. Steffens, K. Tsushima, A. W. Thomas and K. Saito, Phys. Lett. B **447**, 233 (1999).
- [47] W. Melnitchouk, A. W. Schreiber and A. W. Thomas, Phys. Lett. B **335**, 11 (1994).

- [48] F. Gross and S. Liuti, Phys. Rev. C **45**, 1374 (1992).
- [49] W. Melnitchouk, M. Sargsian and M. I. Strikman, Z. Phys. A **359**, 99 (1997).
- [50] I. C. Cloët, W. Bentz and A. W. Thomas, Phys. Rev. Lett. **95**, 052302 (2005).
- [51] A. Accardi, W. Melnitchouk, J. F. Owens, M. E. Christy, C. E. Keppel, L. Zhu and J. G. Morfin, Phys. Rev. D **84**, 014008 (2011).
- [52] J. F. Owens, A. Accardi and W. Melnitchouk, Phys. Rev. D **87**, 094012 (2013).
- [53] F. E. Close, R. L. Jaffe, R. G. Roberts and G. G. Ross, Phys. Rev. D **31**, 1004 (1985).
- [54] S. Simula, M. Osipenko, G. Ricco and M. Taiuti, Phys. Rev. D **65**, 034017 (2002).
- [55] P. E. Bosted and M. E. Christy, Phys. Rev. C **77**, 065206 (2008); M. E. Christy and P. E. Bosted, Phys. Rev. C **81**, 055213 (2010).
- [56] M. Arneodo *et al.*, Phys. Lett. B **364**, 107 (1995).
- [57] D. Drechsel, O. Hanstein, S. S. Kamalov and L. Tiator, Nucl. Phys. **A645**, 145 (1999).
- [58] Y. Kahn, W. Melnitchouk and S. A. Kulagin, Phys. Rev. C **79**, 035205 (2009).
- [59] J. Arrington, W. Melnitchouk and J. A. Tjon, Phys. Rev. C **76**, 035205 (2007).
- [60] J. J. Kelly, Phys. Rev. C **70**, 068202 (2004).
- [61] N. Doshi, J. J. Ethier, S. Malace and W. Melnitchouk, in preparation (2013).
- [62] G. R. Farrar and D. R. Jackson, Phys. Rev. Lett. **35**, 1416 (1975).
- [63] R. Blankenbecler and S. J. Brodsky, Phys. Rev. D **10**, 2973 (1974).
- [64] J. F. Gunion, Phys. Rev. D **10**, 242 (1974).
- [65] S. J. Brodsky and G. P. Lepage, Proceedings of the 1979 Summer Institute on Particle Physics, SLAC (1979).
- [66] S. J. Brodsky, M. Burkardt and I. Schmidt, Nucl. Phys. **B441**, 197 (1995).
- [67] E. Leader, A. V. Sidorov and D. B. Stamenov, Int. J. Mod. Phys. A **13**, 5573 (1998).
- [68] Jefferson Lab Experiment PR12-06-110, J.-P. Chen, X. Zheng, Z.-E. Meziani and G. D. Cates, spokespersons.
- [69] Jefferson Lab Experiment PR12-06-122, B. Wojtsekhowski, G. Cates, N. Liyanage, Z.-E. Meziani, G. Rosner and X. Zheng.
- [70] S. Gerasimov, Yad. Fiz. **2**, 598 (1965) [Sov. J. Nucl. Phys. **2**, 430 (1966)]; S. D. Drell and A. C. Hearn, Phys. Rev. Lett. **16**, 908 (1966).
- [71] D. Parno, M. R. Posik and B. Sawatzky, private communication.
- [72] S. P. Malace *et al.*, Phys. Rev. Lett. **104**, 102001 (2010).

- [73] W. Melnitchouk, talk given at Jefferson Lab Users Town Meeting, Jefferson Lab, March 16, 2012, [http://www.jlab.org/div\\_dept/theory/talks/melnitchouk12\\_townhall.pdf](http://www.jlab.org/div_dept/theory/talks/melnitchouk12_townhall.pdf).
- [74] Jefferson Lab Experiment E12-10-103, G. G. Petratos, J. Gomez, R. J. Holt and R. D. Ransome, spokespersons.
- [75] I. R. Afnan *et al.*, Phys. Lett. B **493**, 36 (2000).
- [76] N. Baillie *et al.*, Phys. Rev. Lett. **108**, 199902 (2012).
- [77] M. Anselmino, P. Gambino and J. Kalinowski, Z. Phys. C **64**, 267 (1994).
- [78] T. J. Hobbs and W. Melnitchouk, Phys. Rev. D **77**, 114023 (2008).